PROBING THE NATIVE STATE OF POLY-PROTEINS BY MECHANICAL FORCE

by

Jian-Yu Chen

A Dissertation

Submitted to the Faculty of Purdue University

In Partial Fulfillment of the Requirements for the degree of

Doctor of Philosophy

Department of Physics and Astronomy

West Lafayette, Indiana

December 2020

THE PURDUE UNIVERSITY GRADUATE SCHOOL
STATEMENT OF COMMITTEE APPROVAL

Dr. Ken P. Ritchie, Chair

Department of Physics and Astronomy

Dr. Sergei Savikhin

Department of Physics and Astronomy

Dr. Martin Kruczenski

Department of Physics and Astronomy

Dr. Andrew Mugler

Department of Physics and Astronomy

Approved by:

Dr. John Finley

Dedicated to my lovely family and girlfriend

ACKNOWLEDGMENTS

To this point that I can complete this thesis, I truly appreciate all the people who helped in my research. Without their help, I couldn't have been able to finish my thesis alone. I would like to thank Prof. Ken Ritchie, my academic advisor, for his kind guidance and useful advice on the road to be a doctor. I am glad that he has led me to explore the great and beautiful field of biophysics since I joined his group in 2016. Whenever I lost direction of my research, he always has a way to let me back on track by his solid grasp of physics knowledge and practical experimental experience. I am thankful to Dr. Yoriko Lill, a former research scientist in Ritchie group, for all the assistance and insight I received from her. I give thanks to Caitlin Gish, a REU program student from the University of South Florida, and Matthew Tao and Frank DiBartolomeo, the undergrad researchers, for the help on building up the setup and running the experiments. I also appreciate my committee members - Prof. Sergei Savikhin, Prof. Martin Kruczenski and Prof. Andrew Mugler for the service and the suggestions on my thesis.

I would like to give a big thanks to my lovely family. As my family, they have been very supportive to me on my pursuit of a doctoral degree. They always show me their positive sides so I could be at ease to deal with my academic work here. Finally, I want to express huge gratitude to my girlfriend, An-Chieh Chen. We have been in a long-distance relationship since I came to America. I feel sorry that I could not have enough time to be with her because of the 12300-km-long distance and 12-hr time difference. But she has been there being with me to get through many hard times. She is my biggest supporter in mental. I would like to thank her support and to say I love her so much.

TABLE OF CONTENTS

LIST OF TABLES

LIST OF FIGURES

LIST OF ABBREVIATIONS

AFM	Atomic Force Microscopy
BSA	Bovine Serum Albumin
B-S transition	B-DNA to S-DNA transition
CCD camera	Charge Coupled Device camera
DD water	Distilled and Deionized water
DMSO	Dimethyl Sulfoxide
DNA	Deoxyribonucleic Acid
FT	Fourier Transform
HPLC	High Performance Liquid Chromatography
LED	Light Emitting Diode
M-O bond	Metal-Oxygen bond
MP	Magnet Position
MT	Magnetic Tweezers
OT	Optical Tweezers
PBS	Phosphate-Buffered Saline
ROI	Region of Interest
TRIS	Tris(hydroxymethyl)aminomethane
WLC	Worm-Like Chain

ABSTRACT

The folding and unfolding processes of poly-protein has been tremendously studied recently. The poly-protein dynamics under an external force can play an important role in addressing the issue of the mechanics of muscle tissue. In this research, we use a single-molecule technique: magnetic tweezers to observe the dynamics of 8-mer poly-protein L under different loads applied and then in different Tris-buffered salines. Our result shows that more protein domains unfold as the force load becomes larger. At 6, 7 and 8 pN loads, the poly-protein is most likely to stay in state 1, 3 and 6 with 1, 3 and 6 domains unfolded, respectively according to the probability distribution. This can be well explained by our constructed free energy-related model. The fit results give protein L parameters of persistence length of 0.4 nm, contour length of 18.8 nm and the unfolding energy of 6.5 kT, all in reasonable ranges based on previously reported literature.

Besides, we also find the dependency of transition rate on force load and salt. The poly-protein has lower transition rate at high force than at low force due to the free energy tilting effect since high force extremely decreases the possibility of protein unfolding that results in a huge drop in the total number of folding and unfolding events. This inverse proportion effect can also be seen in different TRIS-buffered salines (TRIS-150mM NaCl, TRIS-1M NaCl, and TRIS-1M KCl,). We explore the effect of salt concentration, when the concentration of NaCl is increased, the transition rate increases while the probability distribution remains almost the same, indicating the protein unfolding barrier is lowered without altering the overall energy landscape. We attribute this to, first, the charge shielding effect that more interactions between ions and water molecules occur, causing fewer water molecules available to interact with the charged part of protein than before, and, second, more direct interactions of ions with protein that might affect the electrostatic-related transition rate. Considering the effect of salt type, the two 1M alkali metal-chloride salines are compared. We conclude that ions with larger size have less effect on transition rate because ions with smaller size (Na^+) can create stronger bonds with water that increase the interference on the protein interaction with water and can easier penetrate into protein to directly interact with the protein.

CHAPTER 1. INTRODUCTION

Proteins, large molecules composed of one or more long chains of amino acid residues, play a vital role and are an essential part of all living organisms. They perform a variety of functions within our body. They are important for growth and maintenance of tissues. Human bodies use them to build and repair cell tissues, muscles, and organs. In addition, they provide our body with a structural framework. Some proteins are fibrous and provide stiffness and rigidity for cells and tissues. Besides, they take part in many physiological reactions and biological processes. For instance, proteins can serve as a source of energy which provide four calories per gram and make enzymes, hormones, and other body chemicals that human beings need. They can act as a signal messenger that helps communication between cells and tissues. They also participate in DNA replication and transportation of molecules as well. Proteins have many roles in our body. Without them, it is not able for the body to work properly.

Proteins are distinguished from each other in the sequence of amino acids where the order affects the folding route to a tertiary structure that determines its characteristics. The sequence may have several independent subunits called domains, each of that can fold independently into a specific functional three-dimensional stable structure. Many proteins only have a single domain, while others may contain several domains, either the same or different. Single-domain proteins have been studied for several decades. Many properties, such as bond type and its strength, information of transition states, stability, and the folding kinetics of proteins, have been discovered and explained by theoretical calculations or the experimental observation of protein folding and unfolding processes [1-6]. However, so far scientists haven't fully understood the mechanism by which the protein domains evolve and are not able to precisely predict the tertiary structure and its function using the protein sequence [7-10]. For multi-domain proteins, especially proteins with different domain types, it's even more complicated because additional factors have to be considered [11-16]. But it's worthwhile to give it a try because it might help solve more biological secrets by considering the interactions between domains.

As the first project of this research, we look at the energetics of a multi-domain protein under different forces. Understanding the behavior of multi-domain proteins under forces has been gaining importance in recent years because these proteins are regarded as the cause of tissue elasticity and extensibility. For instance, the folding and unfolding of those domains in the protein

titan demonstrate its extensibility and elasticity that greatly affect the functional characteristics of muscle tissue [17-20]. Some multi-domain proteins (talin and vinculin) are also related to cell-cell signaling [21]. Hence, we aim to study how a multi-domain protein reacts under different forces; in other words, how the energy landscape evolves upon change in applied tensile force. To simplify the problem, we only test a protein with all domain types the same. We use an engineered poly-protein that has eight individual protein L's connected to each other in series. Unlike usual protein domains, each protein L is already a complete protein but is used to represent a domain unit in the chain. We use protein L since it is a simple and well-defined protein [22-25]. During experiments, each unit of the multi-domain poly-protein unfolds and refolds individually and the average number of unfolded domains increases as the force increases. Each (un)folding represents a state transition. The poly-protein chain has eight repeats of protein L which means intrinsically there are nine states in total from its natural state with all domains folded to the last state with all domains unfolded. Through a micro-sphere tag technique, we are able to observe the dynamics of the eight-domain poly-protein (jumping among the states) under force. We also construct a theoretical model to fit the experimental results and have a discussion from an energetic point of view.

On the basis of this work, we then seek for other factors that affect the poly-protein performance. Salts are found in living organisms and affect proteins in a variety of ways. They affect protein solubility through changes in salt concentration, for instance, salting in and salting out effects [26-29]. They also act as protein stabilizing and destabilizing agents [28-34], influencing the structural arrangement of protein via electrostatic interactions, thereby affecting its function. Therefore, as the second project, we explore the salt effect (salt type and concentration) on the energy landscape of poly-protein in the folding dynamics.

To complete our projects, a special tool: magnetic spectroscopy technique was used. The setup and the details of the single-molecule manipulation technique will be discussed in Chapter 2. Then in Chapter 3, sample preparation and the protocol of data collection including image acquisition and analysis methods will be covered. Some general cases interpreted from experimental results would be explained at the beginning of Chapter 4. After that, the experimental data and a discussion for each of my two projects: the free energy landscape of poly-protein L under force and the effect of salt on it will be presented in Chapter 4 and 5, respectively. Last, a conclusion with a discussion about the future work is in Chapter 6.

1.1 Recent Advances in Experiment and Theory of Multi-domain Protein (Titin)

Since the advent of force spectroscopy techniques, scientists have taken advantages of the repeatedly mechanical loads to study single molecules for decades. In early 1990's, Prof. Hermann Gaub and his group pioneered the use of atomic force microscopy-based approach for the study of biopolymers and were the first to explore the mechanical properties of protein titin by observing the repeated unfolding and refolding pathways [35]. In early 2000's, Prof. Julio Fernandez's group proposed force-clamp atomic force microscopy technique to solve the problem that the force changes so much during the unfolding of a protein, resulting in a sawtooth pattern. It has been solved by adding a feedback system [36]. Later in late 2000's, Fernandez and his group introduced the magnetic tweezers system for the study of protein folding and unfolding since the ease of application of a constant force [37]. His research majorly focuses on protein titin folding/unfolding dynamics and its role in muscle contraction and elasticity.

To date, titin, a giant elastic protein in human body consisting of 244 individual protein domains, having a molecular weight of 3.0~3.8 MDa, is the best-known multi-domain molecule studied by those force spectroscopy techniques. Due to its diverse domains, one may create different constructs for one's needs by recombining regions of titin using molecular engineering techniques. Some constructs are parts of protein titin that protein domains are linked in their natural sequence of the native molecule, for example, (I24–I25-N2Bus-I26–I27) or immunoglobulin domain series, (I65-I70), and so on [38, 39]. It directly exhibits the characteristics and functions of the protein fragments. Some constructs are so-called poly-proteins that comprises repeats of identical domain units, including two sorts, mono- and hetero- poly-protein, for example, (I69)8 and (I27-I28)4 [40, 41] for mono- and hetero-, respectively, which helps show specific mechanical properties when stretched in force-extension experiments. This unique "fingerprinting" technique along with any force spectroscopy can be used to sort and identify a specific region of a protein or be used for long-time observations [42]. Since the massive research achievements on protein titin, it becomes the landmark for the studies of mechanical properties of other single molecules (e.g. DNA, RNA, ankyrin…) [43, 44], which have been probed in a similar manner.

The related theory comes behind. Rief et al. introduced a two-state model for biopolymer extensibility in 1998 by combining the classical polymer elasticity and the kinetics of a thermodynamic two-level system [45]. Berkovich et al. in 2010 used Langevin dynamics to investigate a force-induced entropic energy barrier to explain the two-state hopping phenomena

that have been observed in stretched proteins [46]. In early 2015, Chen et al. studied tandem modular I27 dynamics but only derived the force-dependent free energy landscape for a single folded and unfolded I27 [47]. Later in middle of 2015, Valle-Orero et al. then followed concepts from Berkovich to construct the free energy landscape for the unfolding dynamics of N tandem domains under mechanical force [48]. However, this model lacks of the experimental evidence. Our free energy model is constructed for any number of protein domains (eight protein L's presented in this study). Our model considers three terms: unfolding energy of a single protein domain, indistinguishable domains, and work done by an applied force and a polymer restoring force. It fits well with the experimental data.

CHAPTER 2. EXPERIMENTAL TECHNIQUE

2.1 Single-Molecule Spectroscopy Technique

In the past thirty years, force spectroscopy techniques have become more and more popular for the study of micromanipulation of biomolecules and the investigation of biological processes because of their wide variety of capabilities. Many different biomolecule manipulation techniques, such as optical tweezers (OT) [49-52], atomic force microscope (AFM) [35, 49, 53-55], and magnetic tweezers (MT) [49, 56-59], have been developed and used to stretch, twist, or unzip biological samples ranging from individual molecules [49, 56, 57, 60-62], to groups of molecules [63-65], to even the whole cell [66-68] for measuring their mechanical properties. Although those techniques play an important role in the biological filed, each one has its own problems measuring the measurements. For example, OT, to trap or manipulate a biomolecule by a focused laser beam, might cause local heating or even damage to the sample because of the high intensity of the laser beam [69,70]. Another problem is its poor selectivity, the laser beam might interact with the particles of the sample near the focus of the trapping laser due to relatively the same change in the refractive index [49]. In the case of AFM, it is also difficult to get rid of the interaction between the tip and the studied molecules. Another common drawback for OT and AFM is the small force range and relatively high minimal force magnitude, which is not ideal to detect biological processes at ~0.1 pico-newton (pN) scale, such as nucleic acid dynamics. Complicated operation procedure and small working space might also result in limitation on measurement of the experiments.

Compared to other force spectroscopy methods, MT has many strengths. First, it is very efficient to generate a force with just an extremely simple-to-implement and low-cost setup. Apart from the conventional force, MT can also allow a straightforward application of torque on the molecule which helps observe the rotational motion of the molecules. In addition, MT setup applies and measures smaller forces in comparison with other methods due to low trap stiffness, and it can work in a wide force range spanning five orders of magnitude from >100 pN down to <10 femto-newtons (fN) [49]. Besides, the system still retains its stability as the magnitude reaches as tiny as tens of fN scale. Last and the most important feature is the specificity. Basically, the

magnetic field doesn't have any effect on biomolecules or fluid chambers. It is highly specific to the paramagnetic beads used for direct observation of the motion of the studied molecules [49].

The biggest problem, however, of MT setup is that it cannot achieve the same sensitivity as some other force spectroscopy techniques could. The precision of a measurement of a general MT is about 5~10 nm in spatial resolution and about 10^{-1} to 10^{-2} seconds in temporal resolution, both of which are one order of magnitude higher than others. The temporal and spatial resolution is restricted by the camera-based tracking system because it limits the detection of very fast or very small motion. Fortunately, the spatial and temporal resolution can be improved to Angstrom level using a high-speed camera [71], if necessary.

MT is a powerful instrument well suited for diverse single molecule experiment because of its low cost, ease of use, and simplicity of implementation, combined with the precision of nanometer in length and of tens of milliseconds in time. With the advent of high-speed camera, this technique becomes even more accurate.

2.2 Experimental Setup

The three major parts of our MT apparatus: a set of permanent magnets with a linear positioning system, a superparamagnetic bead tethered to a glass slide through a single molecule and a bead tracking system. Figure 2.1 depicts the experimental setup of our MT for measuring the dynamics of biomolecules (based on the magnetic tweezers setup of Prof. Julio Fernandez, Columbia University [42]).

First, the pair of permanent magnets (D36-N52; K&J Magnetics) located above the sample and objective can generate a magnetic field gradient directly beneath them. The positioning of the magnets above the sample chamber is controlled by a voice-coil linear-positioning motor (LFA-2010; Equipment Solutions) which allows the magnets to move vertically back and forth over a 10 mm range with a position accuracy of ~100 nm and a moving speed of ~0.7 m/s. Controlling the vertical position of the magnets can control the magnetic gradient strength at the focus of the objective and hence set the pulling force on a magnetic microsphere linked to a poly-protein.

Second, single biomolecules of interest in a fluid chamber are chemically tethered to the bottom glass surface by one end and to a superparamagnetic bead by the other end. The beads are manipulated by the permanent magnets' generated magnetic field gradient.

Finally, the bead tracking system consists of a piezo-mounted microscopic objective, a set of lenses and a CCD-camera (OnSemi PYTHON 1300 USB3 mono industrial camera; XIMEA). Height measurement rely on making a look-up-table of bead images at specific heights relative to the objective focal point which is accomplished through precise movement of the objective relative to a stationary bead through the objective piezo positioner (10 nm accuracy). Through the comparison between the image library and instantaneous images of the bead during extension (see Section 3.3 for details of how this is done), this instrument allows the analysis of the mechanical properties of the bead linked molecule, such as molecular elasticity and/or bond strength.

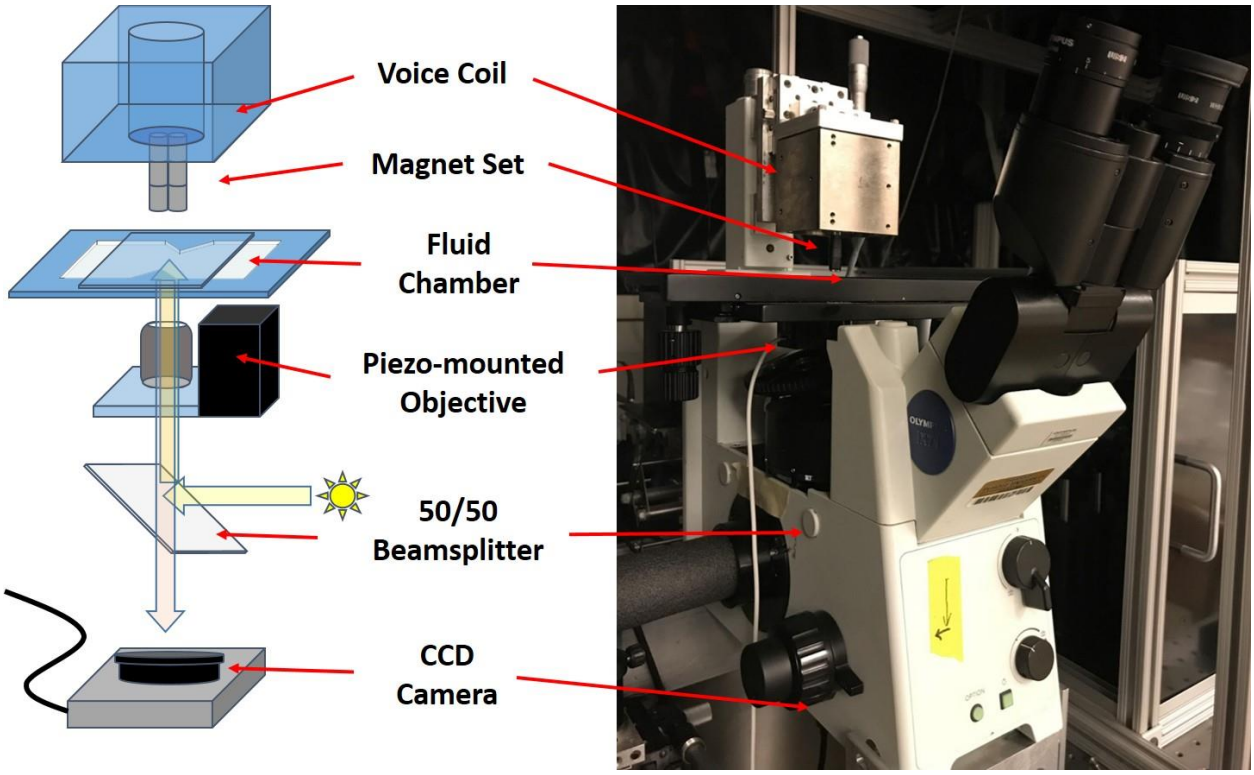

Figure 2.1. A schematic view of MT setup used to measure the dynamics of biomolecules. A stretching magnetic force is applied to tethered superparamagnetic beads through permanent magnet sets whose position is controlled by a voice-coil actuator. LED light is reflected off a 50/50 beamsplitter and shines on the sample through the objective. The reflected light from the sample passes through the beamsplitter and then is recorded via a CCD camera connected to a computer that analyzes the motion of the bead. The piezo is to adjust the vertical position of the objective in the vicinity of its focal plane to help make image library.

2.3 Theoretical Background

2.3.1 Basic Concept

MT is equipped with pairs of permanent magnets that produces magnetic field gradient. We can easily change the applied force strength by moving the relative position of the magnets above the sample. In this section, I will discuss how the magnets apply a force on paramagnetic beads. When a paramagnetic material is inserted into an external magnetic field, the material becomes magnetized. The potential energy U of the magnetized object is described by

$$\mathrm{U} = -\frac{1}{2}\vec{m}(\vec{B}) \cdot \vec{B}\,, \qquad (2.1)$$

where $\vec{B}$ is an external magnetic field and $\vec{m}(\vec{B})$ is the field-induced magnetic dipole moment of the magnetized object, aligning in the same direction as the magnetic field. In a weak field, the dipole moment varies linearly with the field. However, when the field gets larger, it would saturate and reach a maximum value $\overrightarrow{m_{sat}}$ that depends on the properties of the material. The magnetized object in the field then feels a pulling magnetic force defined as the negative gradient of the potential energy. Therefore, when a paramagnetic bead is trapped by a magnetic field, the corresponding magnetic force exerted on the bead by the field can be computed using the equation

$$\vec{F} = -\nabla \mathrm{U} = -\nabla\left(-\frac{1}{2}\vec{m}(\vec{B}) \cdot \vec{B}\right) = \frac{1}{2}\nabla\left(\vec{m}(\vec{B}) \cdot \vec{B}\right). \qquad (2.2)$$

The permanent magnets used in our MT setup are the strongest neodymium magnets (N52). They can reach field strengths as high as 14800 Gauss. In addition, the magnets always move within a small range less than 8 mm from the beads. In this case, the magnetic field is strong enough that we can consider that the dipole moment saturates and approaches a material-dependent maximum value $\overrightarrow{m_{sat}}$. Thus, the bead is assumed to be uniformly magnetized so the dipole moment can be written as

$$\overrightarrow{m_{sat}} = \overrightarrow{M_{sat}} \times V\,, \qquad (2.3)$$

where $\overrightarrow{M_{sat}}$ and V are magnetization and total volume of the bead, respectively. Thus, the force becomes

$$\vec{F} = \frac{1}{2} M_{sat} V \nabla(B) = \frac{1}{2} M_{sat} V \frac{\partial B}{\partial z} \hat{z} \,. \qquad (2.4)$$

The magnets exert an upward stretching force because the gradient of magnetic field is positive along the z direction. For a given magnets position, the force can be considered constant because the length scale of the motion of the bead (~nm) is much smaller than that of the change in the magnetic field (~mm). On top of that, the force can become larger or smaller as the regional gradient increases or decreases when moving the magnets downwards or upwards on the mm length scale.

Why are a pair of magnets rather than a single magnet used in a normal MT setup? Of course a single magnet is able to apply a force on the bead, but it has some problems. At first, it's not easy to control the force direction and strength because the curvature of the field lines make it difficult to align the filed on the center of the objective. A pair of magnets aligning vertically but in opposite directions produce lateral magnetic field from the N pole of a magnet to the S pole of the other over a large area. Those magnetic field lines are mostly parallel to each other so the field gradients over that area point in the same direction over a large area. Therefore, the force applied to the beads in the field of view is basically the same both in magnitude and in direction. Unlike from a magnet pair, the magnetic field from a single bar magnet is parallel to the axis in the middle part of the magnet but curves quickly away from the center. The gradient direction and magnitude would change at different positions below the magnet. That implies the beads would not only feel a vertical force but also be stretched in the horizontal direction. In addition, even in the same field of view, the forces given to the beads are a bit different from one another due to different gradient magnitudes. Thus, the accuracy and precision is much improved with magnet pairs. And last, a single magnet cannot produce torque on the target. But, rotation of the beads can be more easily applied by rotating the magnets when a pair of magnets are employed. (Note that the technique of applying a controlled external torque was not used in the studied presented here.) Now, the remaining problem for the quantitative analysis of the magnetic manipulation is how to measure the applied force.

2.3.2 Force Measurement

The most common way of determining the applied force in magnetic tweeze setups is the quantification of the Brownian motion of a tethered bead in liquid [57]. The thermal fluctuations cause the random deviations of a bead from its equilibrium position in the horizontal plane. Using the equipartition theorem, the potential energy stored in the spring-like polymer-bead system is connected with the average kinetic energy per degree of freedom. The following equation allows the measurement of the stretching force

$$F = \frac{k_B T L}{\langle \delta y^2 \rangle}, \qquad (2.5)$$

where k_B, T, L, and $\langle \delta y^2 \rangle$ represent Boltzmann constant, the temperature of the system, the extension of the tethering molecule, and the variance of transverse fluctuations of the bead, respectively. Thus, in principle, the applied force can be readily computed in real time once we acquire the values for temperature, the length of the tether, and the transverse fluctuations. For a more accurate calculation, however, it is better to analyze the bead motion in Fourier space [57]. The power spectral density of the position of the bead is experimentally acquired and then used to correct the variance of fluctuations due to the instrument vibration and integration time of camera especially under higher forces.

Popa et al. provides another method which applies to our MT to determine the applied force magnitude [42]. By observation of the folding and unfolding processes of protein L-DNA construct, the step sizes of the tested protein L chain and the appearance of the DNA B-S transition are recorded for force calibration. Here is a brief description about how they determined the force. The magnetic field has maximal value at the magnets' surface and then decreases with increasing distance from the surface. They assume the magnetic force decays exponentially as the field does and give a magnet law as

$$F = ae^{-bMP}. \qquad (2.6)$$

Here they introduce worm-like chain model [79] that well describes the behavior of a semi-flexible (stiffer) polymer with consecutive segments all roughly aligned in the same direction, and with persistence length (used to describe the bending stiffness of a polymer) within a few order of

magnitude of the polymer length. A description of force dependence of polymer extension is as follows,

$$F_{WLC}(x; L_c) = \frac{k_B T}{\xi}\left[\frac{1}{4}\left(1 - \frac{x}{L_c}\right)^{-2} - \frac{1}{4} + \frac{x}{L_c}\right], \quad (2.7)$$

where ξ, L_c and x are protein persistence length, contour length, and the observed extension. Then combine the WLC model with the magnet law to get

$$MP(x) = -\frac{1}{b} ln\left\{\frac{1}{a}\frac{k_B T}{\xi}\left[\frac{1}{4}\left(1 - \frac{x}{L_c}\right)^{-2} - \frac{1}{4} + \frac{x}{L_c}\right]\right\}, \quad (2.8)$$

where ξ and L_c are known protein L parameters of persistence length of 0.58 nm and contour length of 18.6 nm. MP is the magnet position, x is the observed step size, and a and b are fitted values for actual data. In order to calibrate this magnet law, a well-known standard force, the B-S transition of DNA molecules, is necessary. For this correction, the above two equations change into

$$F(MP) = F_{B-S} e^{b(MP_{B-S} - MP)}. \quad (2.9)$$

and

$$MP(x) = MP_{B-S} - \frac{1}{b} ln\left\{\frac{1}{F_{B-S}}\frac{k_B T}{\xi}\left[\frac{1}{4}\left(1 - \frac{x}{L_c}\right)^{-2} - \frac{1}{4} + \frac{x}{L_c}\right]\right\}. \quad (2.10)$$

For the experiments, the standard DNA molecule is attached between the protein L chain and the magnetic bead for a reference and the transition happens at a well-defined force of 65 pN. The B-S transition is observed when the magnets are moving to the position of $MP_{B-S} = 0.99 \pm 0.05\ mm$, marking 65 pN for the position. Thus, the only unknown parameter needed to determine in the equation is b, which can be obtained by fitting the equation to the experimental data of step size versus magnet position. From the fitting, they get $b = 0.90 \pm 0.03\ mm^{-1}$. The magnetic force equation then becomes

$$F(MP) = 65 e^{0.9(0.99 - MP)}. \quad (2.11)$$

Furthermore, this force equation is not only useful for a specific material, protein L chain here. If other molecules are placed to be tested, the DNA B-S transition still should be observed when the magnets are at the same height as when protein L is tested. The parameters of persistence length, contour length, and the observed step size in the equation of magnet position might change for different materials, but the parameter b got from the fit should remain the same as long as the setup is stable during the measurements. Currently, we use a calibration determined by the Fernandez group at Columbia University that sets the applied force on the superparamagnetic beads at 4 pN when the magnetics are positioned 4 mm above the sample. The magnets are positioned 4 mm above the sample by a manual micrometer-based translator. The details for magnetic force calibration is in APPENDIX A. Before starting running our projects, we also checked if the observed data (step size) matches the right corresponding applied force, a comparison between our results and Liu's is described in APPENDIX B .

CHAPTER 3. SAMPLE PREPARATION AND DATA ACQUISITION

3.1 Sample Preparation

3.1.1 Overall Description

This section details the preparation of the sample for observation in our magnetic tweezers-equipped microscope. In brief, the sample chamber consists of a fluid-filled chamber constructed of a space sandwiched by two glass coverslips (see Figure 3.1). The bottom coverslip is functionalized to bind one end of the poly-protein under investigation. The free end of poly-protein is biochemically attached to a streptavidin-coated super paramagnetic bead for manipulation in a magnetic field. A non-magnetic reference bead is bound directly to the bottom cover glass to allow for differential extension measurement between the reference and the poly-protein-bound magnetic bead.

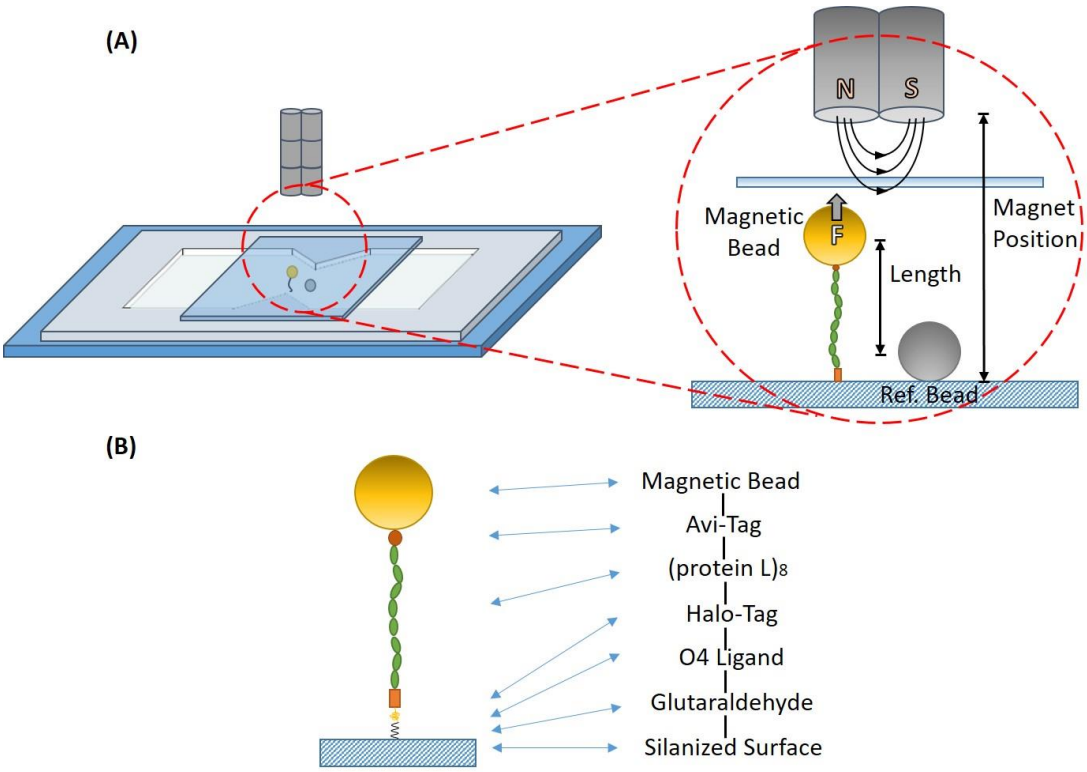

Figure 3.1. An enlarged side view of fluid chamber and surface chemistry. (A) The biomolecule or protein of interest is chemically attached to a glass surface by one end and to a paramagnetic bead by the other end. The molecule is stretched by an adjustable pulling magnetic force given by permanent magnets at different magnet heights. A non-magnetic bead sits next to the magnetic bead for a reference. (B) An amine-silanized glass surface crosslinks to the amine-terminated side of an O4 ligand by glutaraldhyde. An eight repeats of protein L chain with a Halo-Tag at one end and an Avi-Tag at the other end is introduced into the chamber. The Halo-Tag side forms a covalent bond with O4 ligand for anchoring and the Avi-Tag side is chemically tethered to a streptavidin-coated magnetic bead.

3.1.2 Coverslips Surface Cleaning Steps and Surface Silanization

There are two types of coverslips for making the fluid chambers. (Top circle coverslip: 25 mm in diameter, 0.13~0.17 mm in thickness; Bottom rectangular coverslips: 22X24 mm, 0.13~0.17 mm in thickness; both from VWR). Both types of the coverslips are cleaned following the same glass-washing steps. The coverslips are sonicated in detergent solution of 1.5% v/v Hellmanex (Hellma) in distilled deionized water (DD water) at 50° C for 60 minutes and then sonicated in HPLC-grade acetone and HPLC-grade ethanol (both from Sigma-Aldrich) for 30 minutes, sequentially. Between each sonication, wash the coverslips with DD water ten times.

After washing with ethanol, the coverslips are dried with nitrogen gas and baked on the hot plate at ~100◦ C for at least 10 minutes. The top and bottom coverslips are then separately treated with different surface treatments. For the top ones, they are repel-silane treated by immersing them in 10 ml repel-saline solution for 15 minutes, washed with ethanol, dried with nitrogen gas, and baked on the hot plate at ~100◦ C for 15 minutes. The bottom glasses are silanized in a 1% v/v (3-aminopropyl)-trimethoxysilane (Sigma-Aldrich)/ HPLC ethanol solution for 20 minutes, rinsed with HPLC-grade ethanol five times, dried with nitrogen gas, and baked on the hot plate at less than 100◦ C for 120 minutes. The treated top and bottom coverslips are stored dessicated until use. Before using the coverslips, they are baked again on the hot plate at ~100◦ C for 10~15 minutes to make sure there is no moisture on the surface.

3.1.3 Fluid Chamber Fabrication

The fluid chambers are made of a strip of hourglass-shape parafilm sandwiched between the top and bottom coverslips. The chamber is baked on the hot plate at 85◦ C for 15 minutes to melt the parafilm.

3.1.4 Magnetic and (Nonmagnetic) Reference Bead Attachment

To prepare the chambers for observation, a solution of glutaraldhyde (Sigma-Aldrich) 1.5% v/v in phosphate-buffered saline (PBS) is injected into the chamber and incubated for 50 minutes at room temperature. 100 μL of a solution of 2.5~3 μL nonmagnetic reference beads (Spherotech AP-25-10) diluted in 1 mL PBS is added into the chamber and left to react for 15 minutes then washed with 100 μL PBS several times to remove the extra reference beads that didn't stick to the surface. The reference beads give a marker for the position of the bottom coverglass while not being affected by the magnetic pulling force. Height measurements will be performed as differential heights between the reference bead and the poly-protein linked magnetic bead to increase precision and remove global vibrations in the system. The chambers are incubated with a 100 μL solution of 0.85 % w/v HaloTag amine (O4) ligand (Promega) diluted in PBS (2.2 μL 5 mg/mL HaloTag amine (O4) ligand (Promega)/DMSO in 1.3 mL PBS) overnight at room

temperature. After reaction of O4 ligand with the surface, chambers are washed with fresh TRIS blocking buffer (20 mM Tris-HCl pH 7.4, 150 mM NaCl, 2 mM $MgCl_2$ and 1% w/v thiol blocked-BSA (Lee Biosolutions)) several times. Chambers are left at room temperature for at least 5 hours to block those area that didn't react to reduce nonspecific binding of proteins. The chambers can be stored in a 4° C fridge for several days at this point.

On the day of observation, the chambers are washed with fresh TRIS buffer and ~100 μL buffer is left in the chamber. Before the MT measurements, a solution of 0.52 mg/mL protein L is diluted 1000 times in PBS buffer. 3 μL streptavidin-coated magnetic-bead solution (Invitrogen 65305) is added to 500 μL of the diluted proten L solution and is mixed by rotation for at least 10 minutes at 4° C. 20 μL of this magnetic bead solution is added into the chamber just prior to observation. For a long term measurement, vitamin C (ascorbic acid) can be added into the chamber to a final concentration 1 mg/mL. The purpose of the addition of vitamin C is to reduce the chances of protein oxidation leaving long time measurements.

3.2 MT Measurement

To observe the extension of the poly-protein under applied tension, magnetic beads are injected into the chamber fixed to the microscope stage just prior to observation. Within one minute, beads will land on the bottom surface through diffusion, drift, and gravity. We can easily tell the difference between reference and magnetic beads by the color under halogen lamp illumination. Compared to the reference beads, the magnetic beads are a bit yellow (brown) since the absorption spectra of electromagnetic radiation by each of the two types of beads are different. By eye, we select a set of magnetic and reference beads in close proximity (so the video imaging can be performed on a small area of interest allowing for higher frame rates). Preferably, we wish to locate a magnetic bead that just landed on the bottom coverslip. Magnetic beads that lay for a time on the bottom coverslip tend to bind several poly-proteins. For these experiments we must have a single polyprotein bridging the coverslip and magnetic bead.

The reference bead allows for a differential height measurement between the beads and help to remove systematic errors including system vibration and focal drift. The chosen reference bead should be as close to the magnetic bead as possible to get higher frame rate. The frame acquisition rate can achieve an approximate of 1000 frames per second for neighboring beads. After choosing

the beads the magnets are moved to a position 4 mm above the sample. At the beginning of each measurement, we make a z-stack library under the default force for both the magnetic and reference bead, as detailed below. This library allows for fast differential height determinations, so the extension of the poly-protein can be monitored in real time. The magnet position (and hence the applied force) is set by the voice-coil linear positioning motor and is controlled by computer. Because each protein L chain has 8 repeats of protein L in it, if our chosen magnetic bead is linked to a single protein L poly-protein, it should unfold in 8 discrete steps under high (45 pN) tensions over several seconds. Under lower forces the time increases until, at low enough forces, the chain does not completely unfold during observation. The 8-step unfolding under high tension forms a "fingerprint" that allows for certainty we have a single poly-protein linked between the magnetic bead and the cover glass.

3.3 Image Acquisition and Extension Analysis

For the analysis of the MT measurements, one must take the images of the beads under force and map them to height positions determined from the z-stack taken at the beginning of the observation. The image processing requires four major components including: (1) image acquisition of the z-stack library; (2) Fourier transform (FT) of the bead (magnetic and reference) images, (3) a radial profile of the FT; (4) correlation of each radial profile to a height in the z-stack library. The image processing basically follows the procedure in this paper published by Popa et al. [42].

As mentioned above, a z-stack data library has to be built prior to each measurement. The images are captured by a high speed camera and we highlight the selected two beads by roughly having each of the beads centered separately in a 128x128 pixel region of interest (ROI). The two ROIs are later analyzed, which can Fourier transform an image and then calculate the radial profile of the FT. The Fourier transform is a powerful image processing tool that allows an image (or a product) to be decomposed into a sum of sine waves of different frequencies, phases, and amplitudes. In other words, the Fourier transform here is converting the information of a 2D image in the spatial domain to that in the frequency domain. The Fourier image has many advantages. For instance, shifting an image or adding a background intensity to an image won't change the frequency distribution except for the lowest modes which are not used in the analysis. Hence, there is no need to worry about if the beads are centered or the background intensity is the same for each

measurement. As for the high frequency end of the spectrum, this contains the pixel noise and can also be ignored. Intermediate frequencies are thus used to determine the height of the bead. Throughout this transformation, each of the 128x128 pixel ROIs become a 65x128 pixel FT image due to Nyquist frequency limit that is half of the sampling rate above which all information are captured. The program later computes the radial profile for each of the Fourier images using the equation:

$$\mathrm{r} = 4 \cdot \sqrt{(x - x_c)^2 - (y - y_c)^2}\,, \qquad (3.1)$$

where the number of 4 is a scale factor which can zoom in the FT image by a factor of four, increasing the resolution. And r is the radius of a changing semicircle centered at the edge of the 4x zoomed-in FT image. The x and y are the integral pixel positions, and x_c and y_c are the positions of the estimated center of the diffraction-like semicircle pattern. The program in the FT image measures the average intensity of those pixels found at each radius. From this, one gets the radial intensity profile of the Fourier image of each bead at each height of the z-stack. The radial profile provides the best results for r value ranging from 40 to 140 pixels because it filters low and high frequency noise.

During z-stack acquisition, the two radial profiles are recorded every 20 nm for a total distance range of 2.5 μm by stepping the piezo-mounted objective along the vertical direction, as illustrated in Figure 3.2. The image stack library would provide the information of the considered beads at the known distances away from the focal plane so later it allows comparison of a beads image with the image library to get the z positions of the beads. This is accomplished by first, computing the Pearson correlation between a beads image and the stack library which shows the strength of a linear association between them. Second, make a plot of correlation versus z position and apply a Gaussian fit to this plot. The peak of the Gaussian fitting will indicate the vertical position of the bead. Both the reference and magnetic beads are measured by the program at the same time and the difference between the two peaks gives a measure of the length (extension) of the molecule. From this, we record the extension of the molecule at the frame rate the camera acquires images.

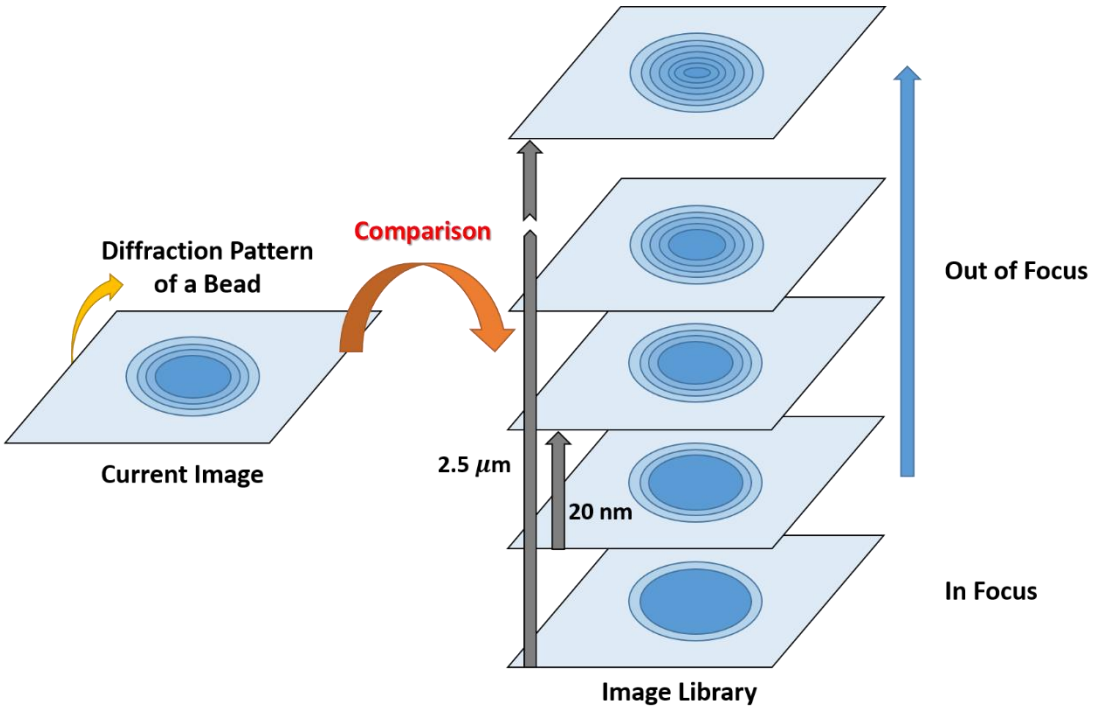

Figure 3.2. Principle of the vertical length measurement. Only a bead pattern is drawn in each image for simplification. The image library has to be built prior to measurement. The diffraction pattern of the studied bead is recorded every 20 nm for a total range of 2.5 μm. By comparing real-time image to the image stack library, the pattern information at the known height away from the focal plane is used to determine the bead position which tells the stretched length of the protein. During real experiments, one magnetic bead and one reference bead need to be recorded at the same time. The reason for that is the image pattern of the reference bead helps get rid of the system vibration and the focal drift.

CHAPTER 4. FREE ENERGY LANDSCAPE OF OCTMER POLY-PROTEIN L

In this chapter, I will discuss the first project: studying the energetics of poly-protein L dynamics under the application of forces and its evolution upon change in force. I will first cover the methods we used for this project, then focus on how the theoretical model was constructed as well as the experimental outcomes, and last have a comparative discussion between the experimental and theoretical results.

4.1 Methods

The sample preparation and experimental methods used in this study are mentioned in Section 3.1 and 3.2. The extension raw data was collected using the program discussed in Section 3.3. The analysis methods are given in next section.

4.2 Data Analysis

4.2.1 Typical Extension Curves and Their Interpretation

Before we start discussing our main results, in this section I will show several time traces of our extension data and interpret what these tell us about the sample under observation. For each plot, it shows the measured differential length between the magnetic and non-magnetic beads. The blue and red lines represent this differential length the magnetic force, respectively. A moving-average filter is applied to the data to smooth it and guide the eye, continuously computing the average of the data in a moving 200-pt window, giving the black line.

There are four very common cases that happened during the measurements. First, the magnetic bead gets completely stuck to the bottom glass surface. Figure 4.1 shows the measured extension for a stuck magnetic bead at different forces. In this case, the position of the magnetic bead is almost independent of the forces, which means the relative position between the reference bead and the magnetic bead remain the same as the magnets get closer to the chamber. As shown in the graph, the stretched length (blue line) is almost flat no matter how large the force (red line) is. This might be because the bead directly attaches the surface through a nonspecific binding that

is too strong to be pulled up or there are too many protein chains binding to the bead that allows any of the chains to extend ate these forces.

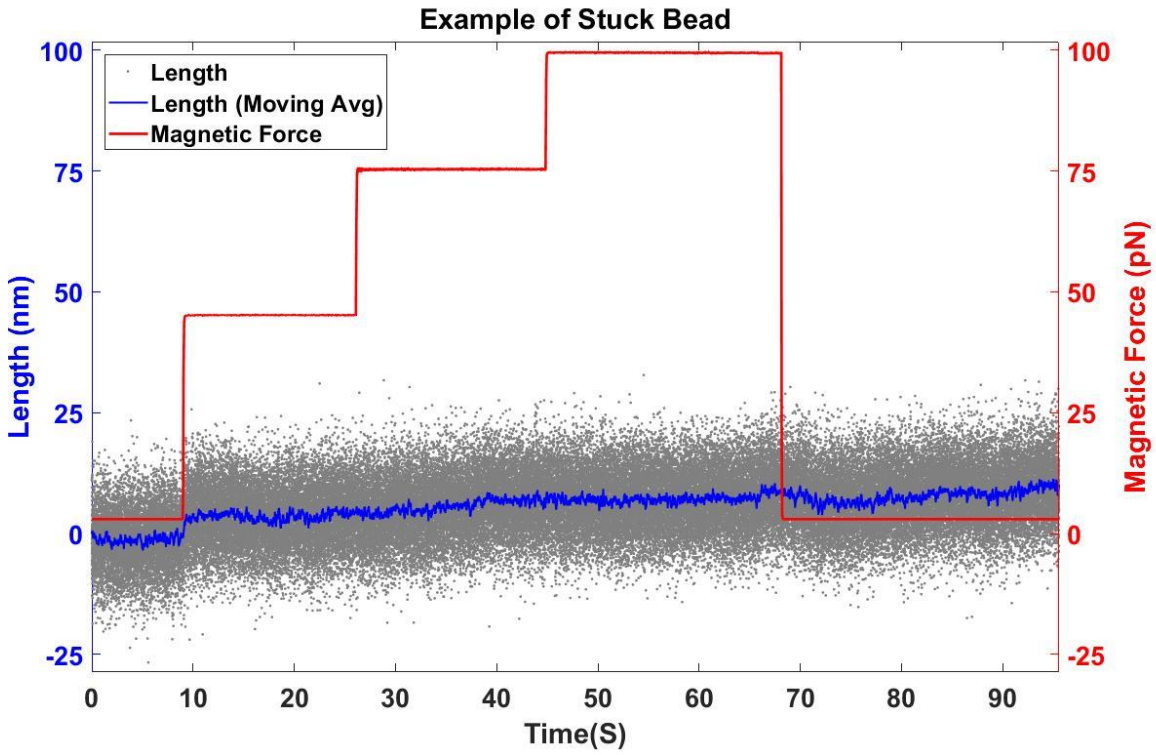

Figure 4.1. An example of stuck bead. The length of the protein L chain is almost constant at different forces because the magnetic bead is completely stuck to the glass surface. The reason for this is that either the interaction between the bead and the surface is too strong or there are multiple protein chains binding to the bead.

The second case is that in the Figure 4.2 we can see a huge step (usually more than 150 nm) when a higher force is applied on the magnetic bead and the bead keeps going up until a lower force is applied. It means something is extended more than 160 nm at the beginning, and the force keeps stretching it with no obvious steps appearing. I expect this is a molecule other than a protein L chain that attaches the bead because it does not contain the 8 step “fingerprint’’ expected for the poly-protein. Also, we expect a maximum extension of approx. 160 nm for an 8-mer of protein L and this molecule clearly extends beyond that.

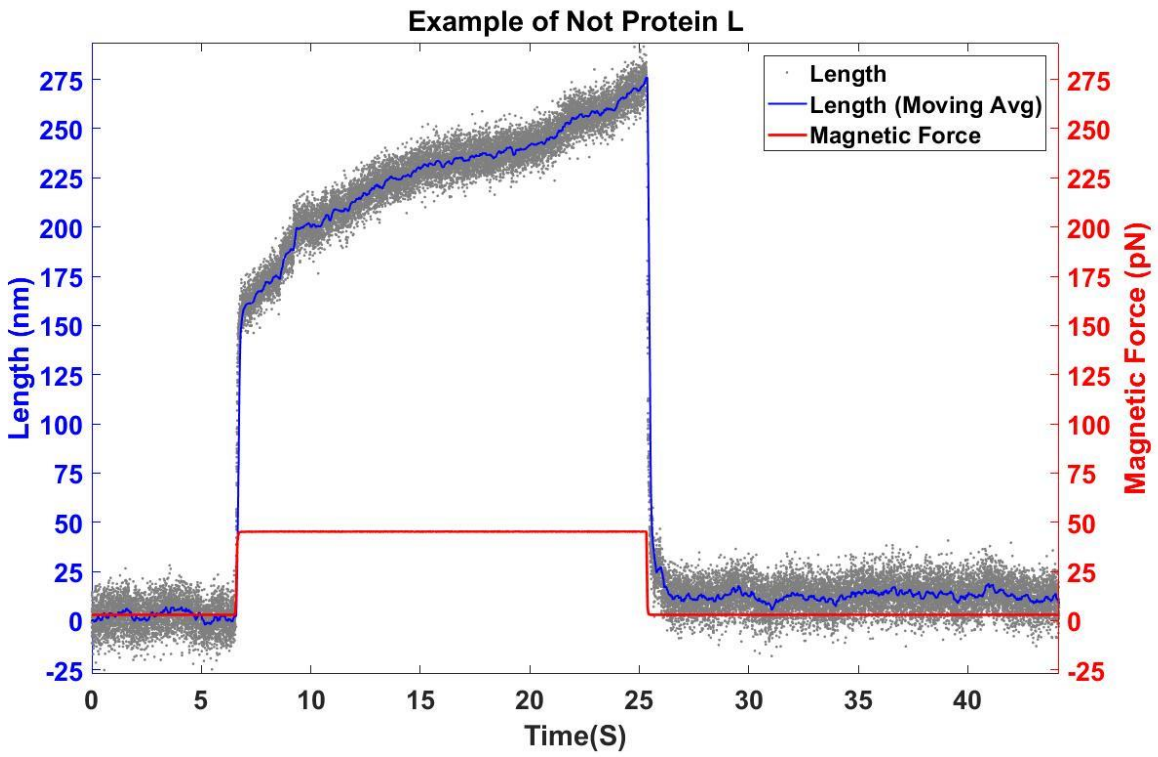

Figure 4.2. An example of not protein L chain. A higher force extends the molecule by more than 160 nm at the beginning and keeps stretching it until the lower force is applied. The force is stretching other molecule rather than the protein L chain because the extension curve is different from the way that a normal protein L chain is extended.

The third case shows the expected trace for the folding and unfolding of a protein L chain. There are 8 repeats of protein L along the chain, so in the plot we should be able to observe 8 unfolding steps as a higher force is given to the magnetic bead. Figure 4.3 shows the unfolding/folding cycles of an anchored protein L chain under three forces, 3 pN, 45 pN and 6 pN. When given a 45 pN test force, we can see in the left plot, the protein domains start to unfold from the native state (all domains folded) to the completely unfolded state in 30 seconds under this force and then re-fold as the force goes back to 3 pN. We may repeat this cycle several times and at any time throughout an observation to confirm we still have a single protein L poly-protein bound. After that, I set the force to 6 pN and observed the extension variations for more than ten minutes. In the right plot, we can see the bead jumping mostly among the first three unfolding states with some short excursions to the totally native state. The measure extension acts the way that we expect for a single 8-mer protein L.

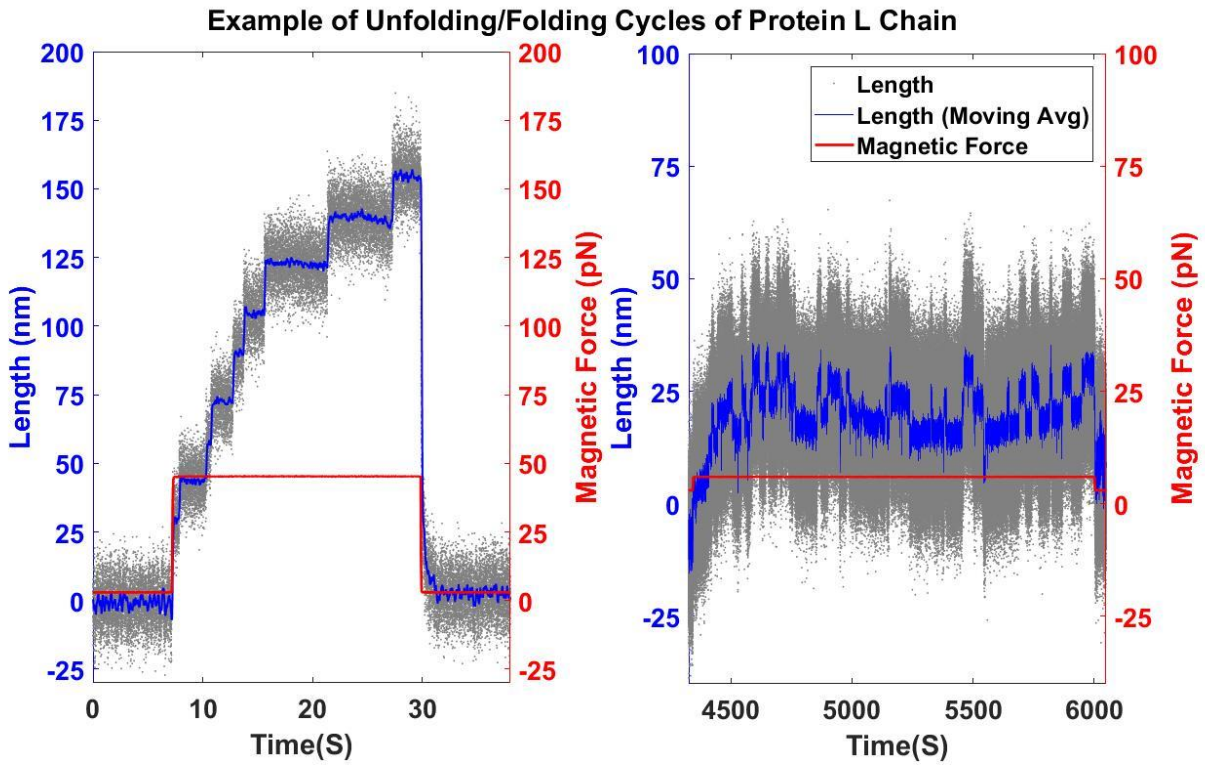

Figure 4.3. An example of unfolding/folding cycles of an anchored protein L chain. The forces applied to the bead are 3 pN, 45 pN, and 6 pN. The 45 pN force unfolds 8 domains (shown in the left view) of the protein L chain and they fold again when a small force (3 pN) is applied. After several cycles of unfolding/folding processes, each state of the protein chain become less noisy than before and we can start the measurements. Later fix the force at 6 pN, the protein chain starts to unfold from its native state. See the bead jump back and forth mostly among the first, second and third states and never goes to the higher state or barely goes back to the native state.

Last case is that we may see more than eight unfolding steps, most likely because more than one protein chain is binding to the magnetic bead. The step sizes are smaller than the expected size that corresponds to the assigned magnetic force since the extra chains dilute the force on each of the chains. Figure 4.4 is an example of multibinding of the protein L chains. There are about twenty steps under a force of 65 pN and the measured step sizes are about 5~6 nm, which is smaller than expected under this force magnitude. We expect that curves like this represent the binding of 2-3 chains to the magnetic bead. In this study, we only use poly-proteins that were tested to have 8-step “fingerprint” under 45 pN load.

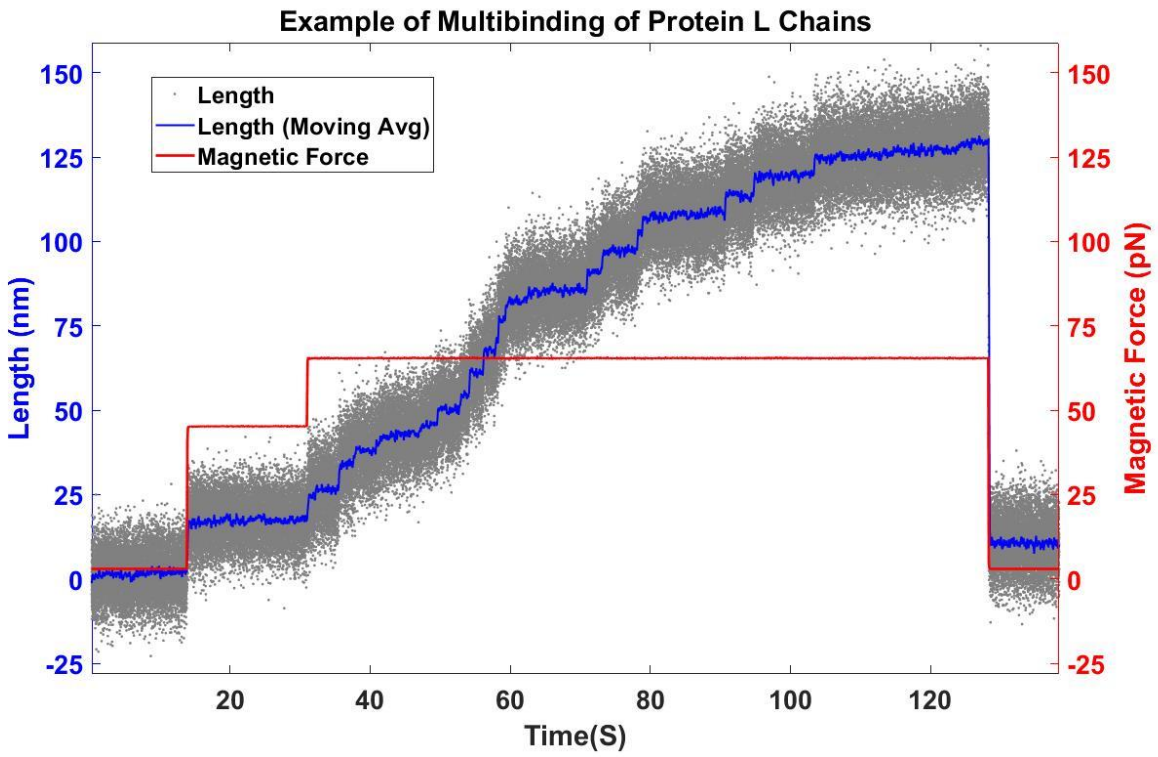

Figure 4.4. An example of multibinding of protein L chains. There are more than eight obvious unfolding steps, indicating that more protein L chains other than one are tethered to the magnetic bead. The corresponding step sizes under a force of 65 pN are smaller than expected, also showing the evidence that more than one chain is binding to the bead at the same time.

Note that after several rounds of measurements, we might observe only six or seven steps for a sample that first displays 8 discrete steps. This is due to protein oxidative damage and occurs usually after several ~10-minute-long measurements. Oxidative damage occurs when the amino acids of an unfolded protein domain react with reactive oxygen species (ROS) in the median. This reaction irreversibly modifies the protein domain such that it is unable to refold properly [72-74]. We add vitamin C to our chambers to minimize this damage [73, 75, 76].

4.2.2 Baseline Subtraction

The whole procedure of baseline removal is shown in Figure 4.5. A 200 pt. moving-average filter (Matlab fn: movmean) was applied to the raw data to smooth it and guide the eye (Figure 4.5(a)). The data was then flattened by removal of calculated baseline as follows (Figure 4.5(b)). First, a change-point-seeking function (Matlab fn: findchangepts) was applied to find abrupt changes in the extension sequence (The arrows denote the positions of change points.). Second, an average of the extension data between each two consecutive change points was calculated throughout the data. Third, differences between adjacent average numbers were calculated and a threshold was set for the differences along the array. For every gap larger than the threshold, the difference was subtracted from the extension data after the transition to continuously connect to previous line. For example, the green part of the smoothed data is shifted down to remove the gap with previous line and then becomes a portion of the non-gap rough baseline. Lastly, the final baseline was constructed by applying another moving average filter (window size of 20000 pts) to this rough baseline (Figure 4.5(c)). This smoothed baseline was then subtracted from the raw data. The corrected data was obtained (dark-blue line in Figure 4.5(d)).

4.2.3 State Determination

For corrected data, the states of the poly-protein could be clearly pointed out (see the labeling in Figure 4.5(d), state n representing the poly-protein has n unfolded domains). One may easily determine them by looking at the extension. The states with the same number of unfolded domains would roughly stay at the same height and the extension is linearly proportional to the number of unfolded domains in the poly-protein since the protein domains are assumed identical and hence the unfolding/refolding step sizes under a force load would be identical.

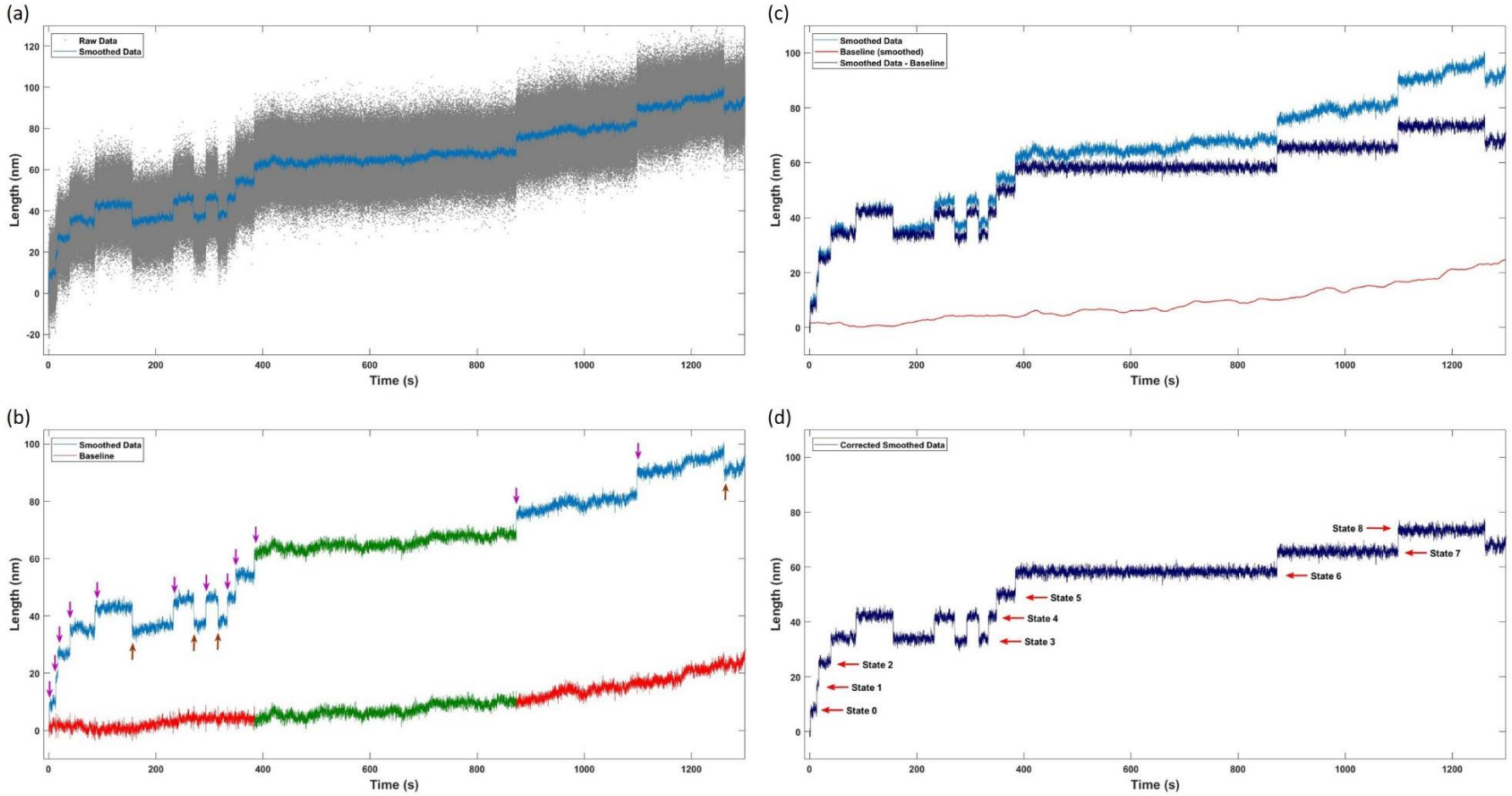

Figure 4.5. Procedure of getting a flattened data. (a) Raw data and smoothed data (moving-average filter applied). (b) A rough baseline is obtained by subtracting the differences (transitions) from the smoothed extension data. The positions of arrows show when the transitions happen during measurement and the directions of arrows indicate the directions of shifting for removing the gaps. (c) The flattened extension data could be acquired by subtraction of smoothed baseline (applying moving-average filter again, window size of 20000 pts) from raw extension data. (d) The states of the poly-protein could be easily determined by looking at the extension height. The extension is proportional to the number of unfolded protein domains in the poly-protein.

4.3 Theory Construction

We designate the state of the 8-mer poly-protein L by the number of unfolded domains in the poly-protein, n. We consider all domains equivalent and model each of them as a simple two-state system with an energy difference ΔE_u between the folded and unfolded state. Upon application of a constant external force, F_M, provided by our magnetic tweezers, work $\int_0^x F_M \cdot dx$, is done to extend the length of the polyprotein to length x in the direction of the force and hence lowers the energy of the system by $-\int_0^x F_M \cdot dx$ [77, 78]. The poly-protein, including its linker and any unfolded domains, opposes this force as a worm-like chain (WLC) of maximum extension, $L_c = L_0 + nl$, where L_0 is the linker length and l is the unfolded length of a single domain. The force required to extend a WLC of maximum length L_c to length x is [79]

$$F_{WLC}(x; L_c) = \frac{k_B T}{\xi}\left\{\frac{1}{4}\left(1 - \frac{x}{L_c}\right)^{-2} - \frac{1}{4} + \frac{x}{L_c}\right\}, \qquad (4.1)$$

where k_B, T and ξ are the Boltzmann's constant, the absolute temperature and the persistence length of the polymer chain, respectively.

Taken together, the free energy of the N-mer polyprotein in state n under applied force F_M at extension x, is

$$H_n(x) = n\Delta E_u - k_B T \ln\left(\frac{N!}{n!\,(N-n)!}\right) - \int_0^x (F_M - F_{WLC}(x'; L_0 + nl)) \cdot dx' \qquad (4.2)$$

where the second term in the free energy takes into account the assumption of identical domains. Figure 4.6 shows this free energy for each state of an 8-mer polyprotein under an external forces of 3, 6, 7 and 8 pN (using the following parameter for illustration: persistence length 0.4 nm, contour length 18.8 nm, energy to break one domain 6.5 kT, and contour length for all linkers 75nm). The dashed lines are the energy curves drawn according to Eq. (4.2) corresponding to states with n protein domains unfolded. One expects transitions between these states to pass

through a high energy transition state which has not been modeled here that would affect the dynamics of the transitions.

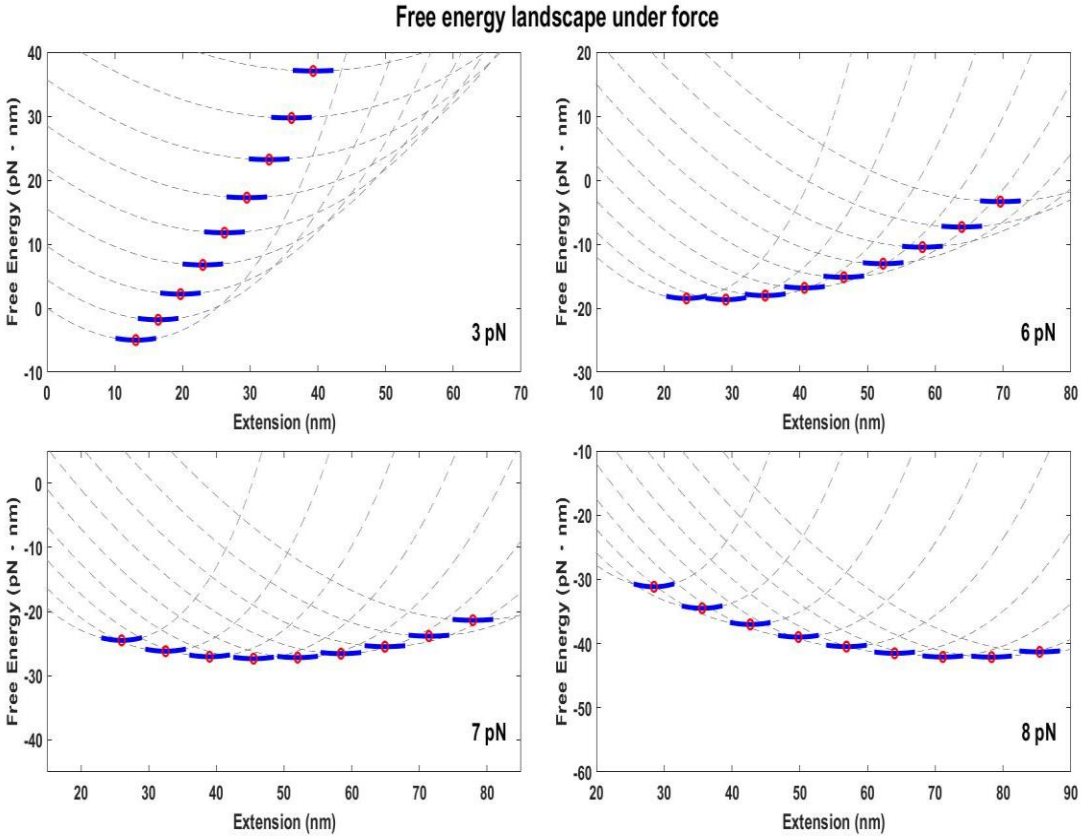

Figure 4.6. A series of energy landscapes of poly-protein L under different external pulling forces of 3pN, 6pN, 7pN and 8pN are plotted using Eq. (4.2) with protein L parameters of persistence length, contour length, energy to break one protein and contour length for all linkers being 0.4 nm, 18.7 nm, 6.5 kT and 75 nm, respectively. Each plot has nine different curves representing all possible states from all protein domains folded to all domains unfolded. As we can see, the higher the force is, the more tilted the landscape is. The blue lines shows the most probable region where the protein chain stays and red circles are the minima (the most stable point) for those curves.

4.4 Experimental Results

Extensions of the 8-mer Protein L poly-protein were observed under applied magnetic forces of 6 pN, 7pN, and 8 pN. Figure 4.7 shows the typical extension over time for the poly-protein under these forces. The applied force (green line) was set at 3 pN prior to extension in all cases. Under this force load, no unfolding events were observed. Upon jumping the force to the final load, there is an initial stretch (red line) of the poly-protein due to extension of the poly-protein without

unfolding of any domains. Subsequent to the initial stretch, the poly-protein undergoes quantized steps under load that increase or decrease its maximally extended length signifying the unfolding/refolding of individual protein L domains, respectively. We label each state of the poly-protein by the number of domains unfolded in that state, which is assigned by counting the steps that increase/decrease the length relative to the end point of the initial stretch (state 0, completely folded poly-protein). Note that we assume all protein L domains are equivalent and thus we do not distinguish which specific domains are unfolded in any state. Upon increase in force, three things are observed. 1) The step size increases for unfolding events. At 6, 7 and 8 pN the step sizes are 7.36 ± 0.08, 7.91 ± 0.17 and 8.60 ± 0.12 nm, respectively (Figure 4.7). Note that each of these values is the average for the trajectories shown in the figure. The step sizes averaged out over multiple trajectories (refer to step size versus force curve in APPENDIX B) are 7.47 ± 0.24, 8.20 ± 0.15 and 8.55 ± 0.13 nm at 6, 7 and 8 pN, respectively. 2) The frequency of transitions between states decreases. At 6, 7 and 8 pN, the transition rates (number of unfolding/refolding transitions in a period of time) are 0.072 ± 0.009, 0.035 ± 0.006 and 0.011 ± 0.001 Hz, respectively (we will discuss this in Chapter 5). 3) The most likely state shifts to one with more domains unfolded. At 6, 7 and 8 pN loads the most likely states are state 1, 3 and 6 with 1, 3 and 6 domains unfolded in the poly-protein, respectively. Analysis of the total time spent in each state relative to the total observation time gives an estimate of the probability of finding the poly-protein in each state under a given load.

Table 4.1 lists the average probability of finding each state of the 8-mer of protein L under application of 6, 7 and 8 pN force loads and Figure 4.8 plots these probability distributions. In this figure we can easily observe the shift to higher average number of unfolded domains under increasing load. These probability values imply the free energy of each state of the system while the varying transition rates under varying load imply the sizes of transition state energy barriers between system states.

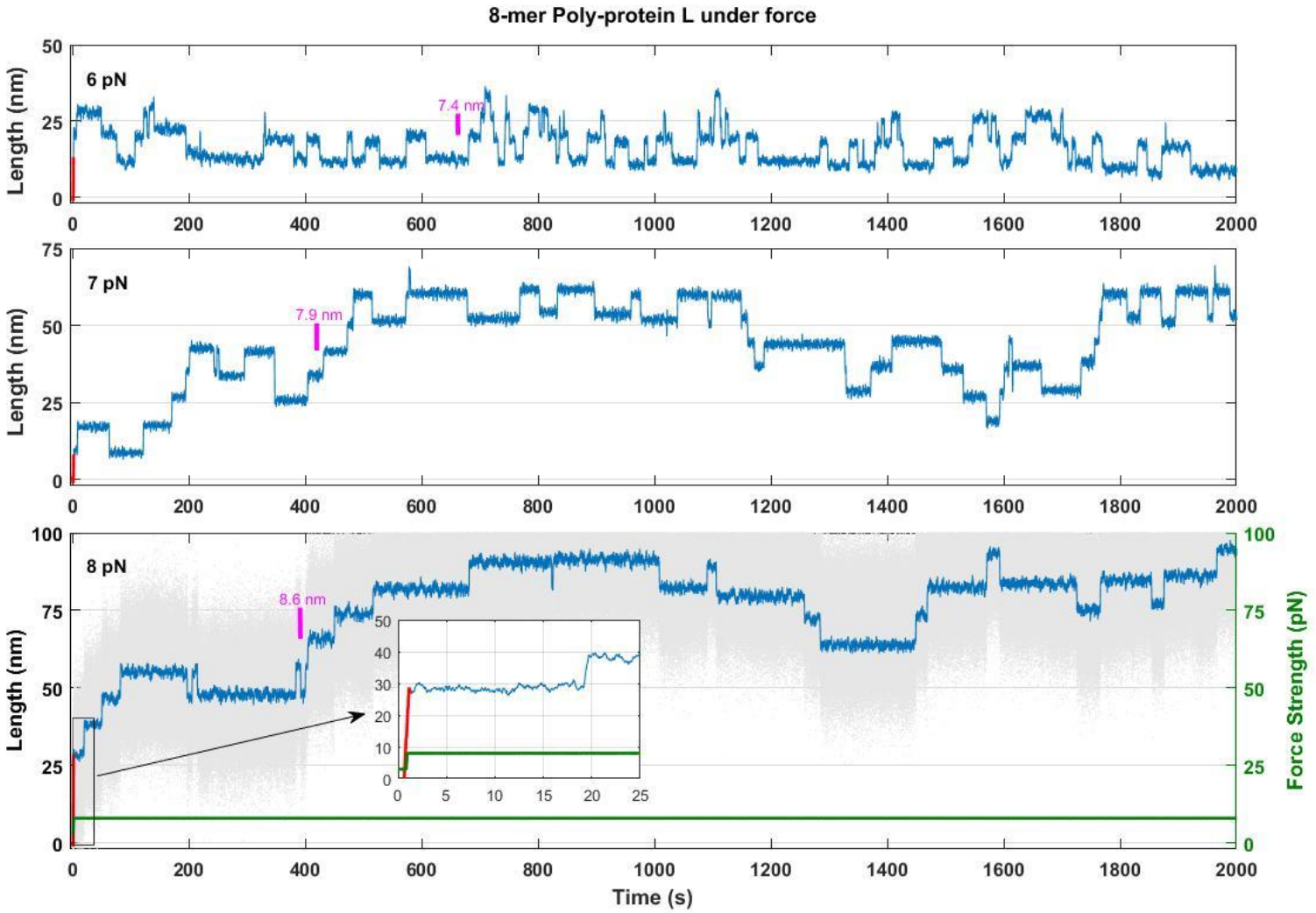

Figure 4.7. Trajectories of unfolding dynamics of 8-mer poly-protein L recorded at different forces (6 pN, 7 pN, and 8 pN). Those trajectories show the poly-protein jumps stepwisely back and forth among states from the fully folded state to the fully unfolded state. The red line represents the initial extension due to increase of force load and the step size increases with increasing force. Our task is to find out the probability of the poly-protein being at each of the nine states under different forces.

Table 4.1. Probability of staying at each step of the poly-protein L at different forces.

Force / # of unfolded proteins	6 pN	7 pN	8 pN
0	0.326 ± 0.107	0.027 ± 0.013	0
1	0.380 ± 0.042	0.095 ± 0.025	0.003 ± 0.003
2	0.214 ± 0.052	0.184 ± 0.062	0.017 ± 0.009
3	0.067 ± 0.025	0.228 ± 0.017	0.046 ± 0.021
4	0.012 ± 0.007	0.214 ± 0.019	0.065 ± 0.022
5	0.001 ± 0.001	0.136 ± 0.029	0.129 ± 0.040
6	0	0.095 ± 0.039	0.305 ± 0.084
7	0	0.020 ± 0.025	0.257 ± 0.055
8	0	0	0.179 ± 0.108

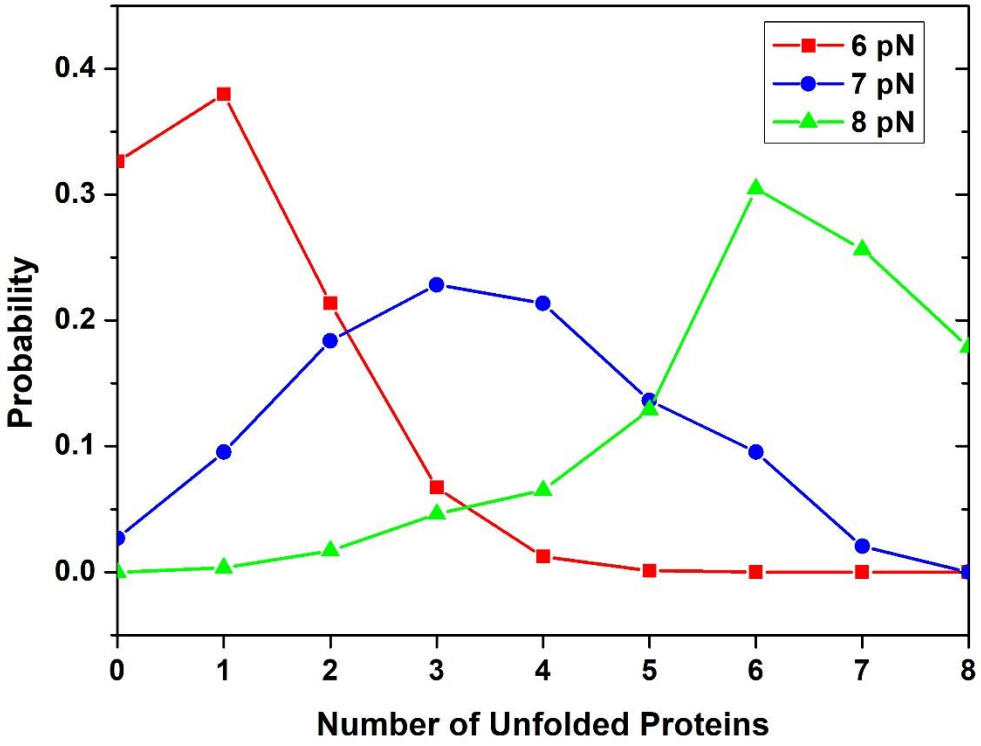

Figure 4.8. The probability distribution of poly-protein L at different forces. The peak goes to the right when a higher force is applied that means the poly-protein prefers the states with more protein domains unfolded as force increases.

4.5 Discussion

To inspect if our theory for the energy landscapes of poly-protein works, we had to find out the theoretical probability value of each state. We first determined the most likely energy that the poly-protein would like to stay for each of the nine states by finding the local minima in the free energy diagram. We then were able to calculate the probability distribution according to the energy-dependent Boltzmann distribution equation given by

$$\frac{P_f}{P_i} = e^{-\Delta E/k_B T} \qquad (4.3)$$

where P_f and P_i represent the probabilities at final and initial states, ΔE is the energy difference between the two states, and $k_B T$ is the thermal energy. We could set the fully folded state as a reference (P_0 and E_0) so the equation becomes $P_f = P_0 e^{-(E_f - E_0)/k_B T}$. The probabilities for the states with any number of unfolded domains could be found by plugging those local minimum energies (red circles in Figure 4.6) into the equation and the normalized probabilities would be the theoretical values.

For the free energy landscape simulation, we used the least squares method, testing persistence length, contour length and the energy for unfolding a protein domain ranging from 0.35~0.6 nm, 18.5~19 nm, and 6~8 kT, respectively. The best fit for the experimental data was acquired with persistence length of 0.4 nm, contour length of 18.8 nm (both in acceptable ranges [37, 48]) and the unfolding energy of 6.5 kT. The unfolding energy is also a reasonable number. An application of magnetic force tilts the free energy landscape and starts to unfold protein L at 4 pN associated with the unfolding step size of about 6 nm. This implies the change in free energy roughly equals the work done by the force which is around 24 pN · nm or 6 kT. Figure 4.9 compares the experimental and theoretical results. As we can see, the simulation results (red lines) basically match the real data (blue lines), especially at 6 pN, and follow the trend that the curve goes to the right when force gets stronger. We believe the fit would become better if we collect more data.

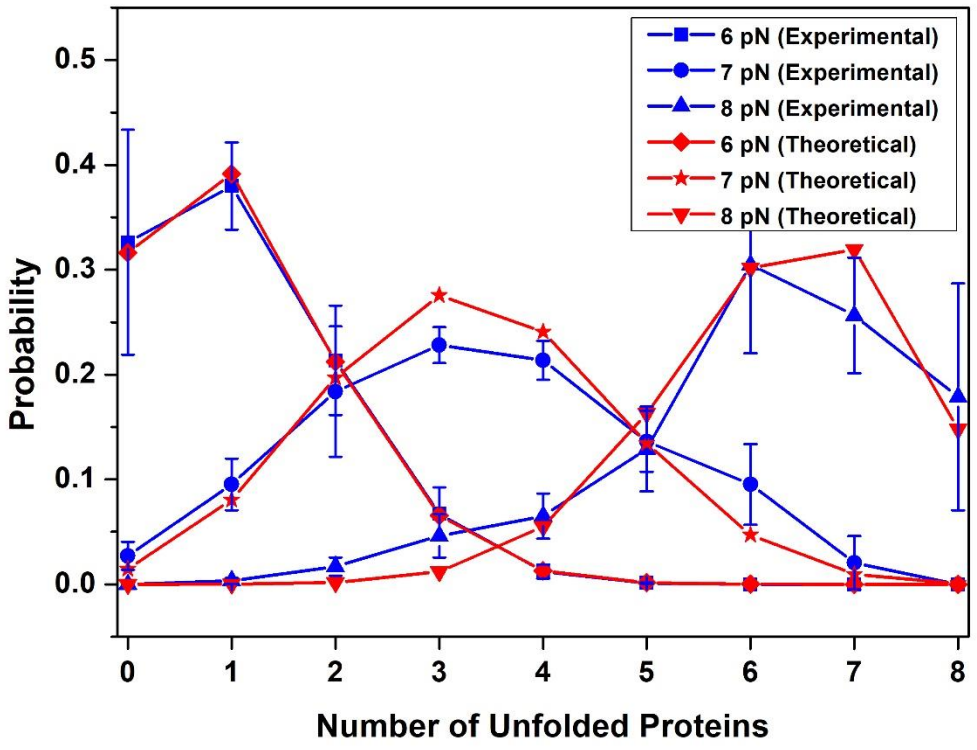

Figure 4.9. Comparison of experimental data and theoretical calculation. Apparently, the theoretical result fits the experimental data well. The poly-protein L prefers staying at states with 0 to 1 unfolded domains, 2 to 4 unfolded domains, and 6 to 7 unfolded domains at 6 pN, 7 pN, and 8 pN, respectively for both experimental and theoretical results.

CHAPTER 5. SALT EFFECTS ON POLY-PROTEIN DYNAMICS

From the results of the first work, we have already known some basic concepts of the poly-protein performance under force. We also desired to know if there are other factors that affect the unfolding energy landscape. The first factor we tested was salt. We tested salt concentration and salt type. In this chapter, I will focus on the experimental results and discuss how salt affects the poly-protein dynamics under force.

5.1 Methods

5.1.1 Materials and Experiment

In this work, the sample preparation is described in Section 3.1 with slight modification. We prepared three different salt solutions. The first one was the normal TRIS-buffered saline containing 150 mM NaCl. The second one was of the same ingredient but the NaCl concentration was increased to 1 M. The last one had salt replaced with KCl but the salt concentration remained the same as the second solution. The rest of the preparation was the same as before and the same MT measurement procedure went through this project. It should be noted that each chamber was only dealing with one type of solution during measurement to avoid the contamination from the previous residue.

5.1.2 Analysis Protocol

The analysis methods as described in Section 4.2 was used for this work. In brief, the raw data was smoothed first by a moving-average filter and then flattened by removal of the baseline that was obtained as described earlier. The flattened data were analyzed to find the probability of a poly-protein at a given state by adding up all the time lengths being at that state divided by the total measurement time. In this work, I also calculated the transition rate between states for each of the three solutions under each tension applied by finding the total number of transitions (total number of unfolding and refolding) over the total time.

5.2 Experimental Results

To test the effects of salt on the construct of eight repeats of protein L, the poly-proteins were observed in three different TRIS-buffered saline solutions (normal TRIS buffer, TRIS-1M NaCl buffer, and TRIS-1M KCl buffer) under different applied forces. In this project, we can examine the factors of both the salt concentration and salt type. The data used for the normal TRIS buffer test are from previous work (see Chapter 4). The first look at this work is the time traces that give the direct observations of poly-protein performance. Figure 5.1-Figure 5.3 depict the time traces of a single poly-protein L in the three TRIS-saline solutions under a force of 6 pN, 7pN, and 8 pN, respectively. For the data collection, each case was repeated more than five times, but in these figures, only one of the time traces was selected to represent for each case. The average performance (probability and its uncertainty) of poly-proteins at different conditions is listed in Table 5.1. The probability distributions for all the nine conditions are illustrated in Figure 5.4.

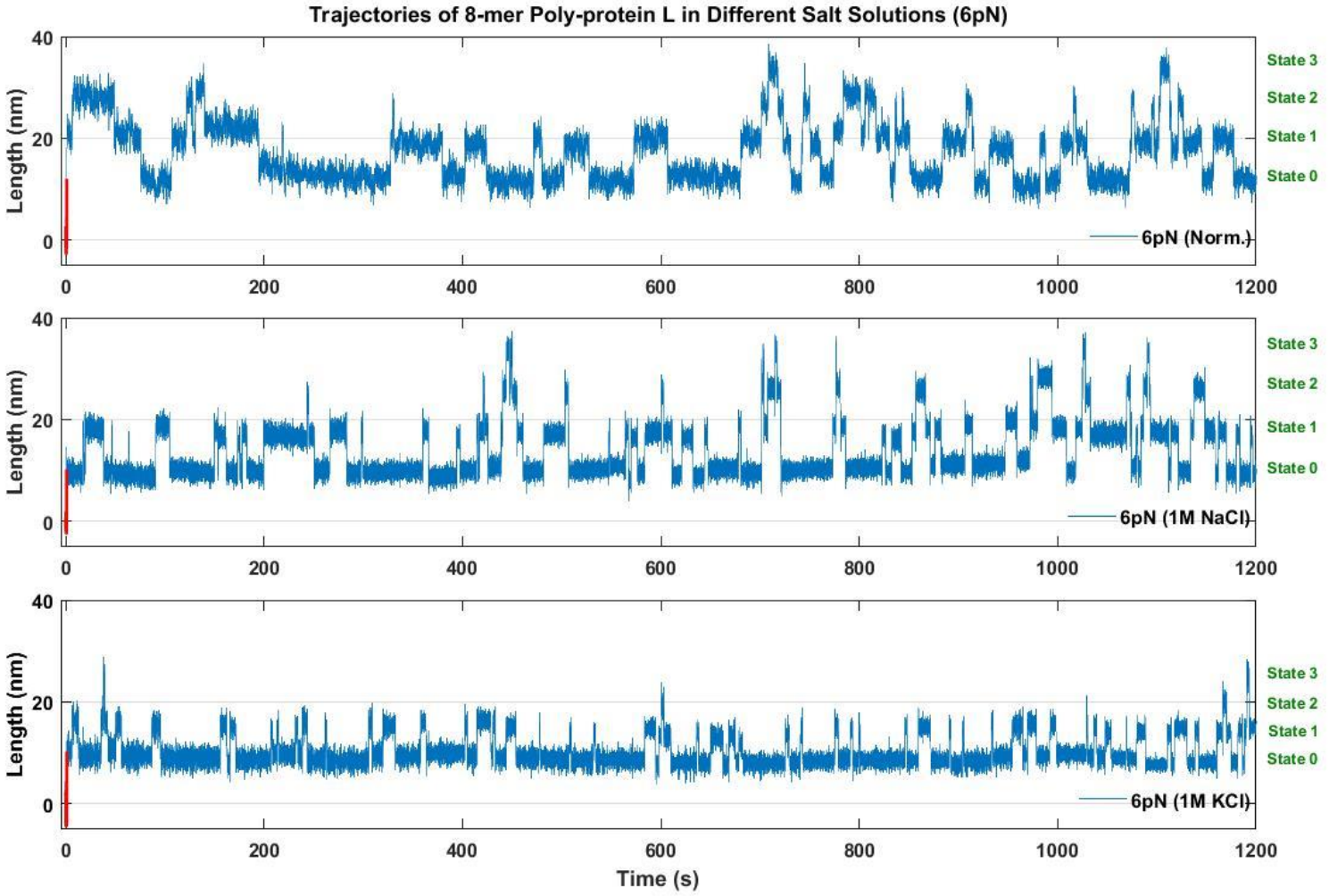

Figure 5.1. Time traces of a single 8-mer poly-protein L in three TRIS-buffered saline solutions at 6pN. Red lines are initial extension due to a rapid increase in force. The transition rates are 4.309 ± 0.513, 5.394 ± 0.226 and 5.588 ± 0.153 (1/min) in normal TRIS, TRIS-1M NaCl, and TRIS-1M KCl buffer, respectively.

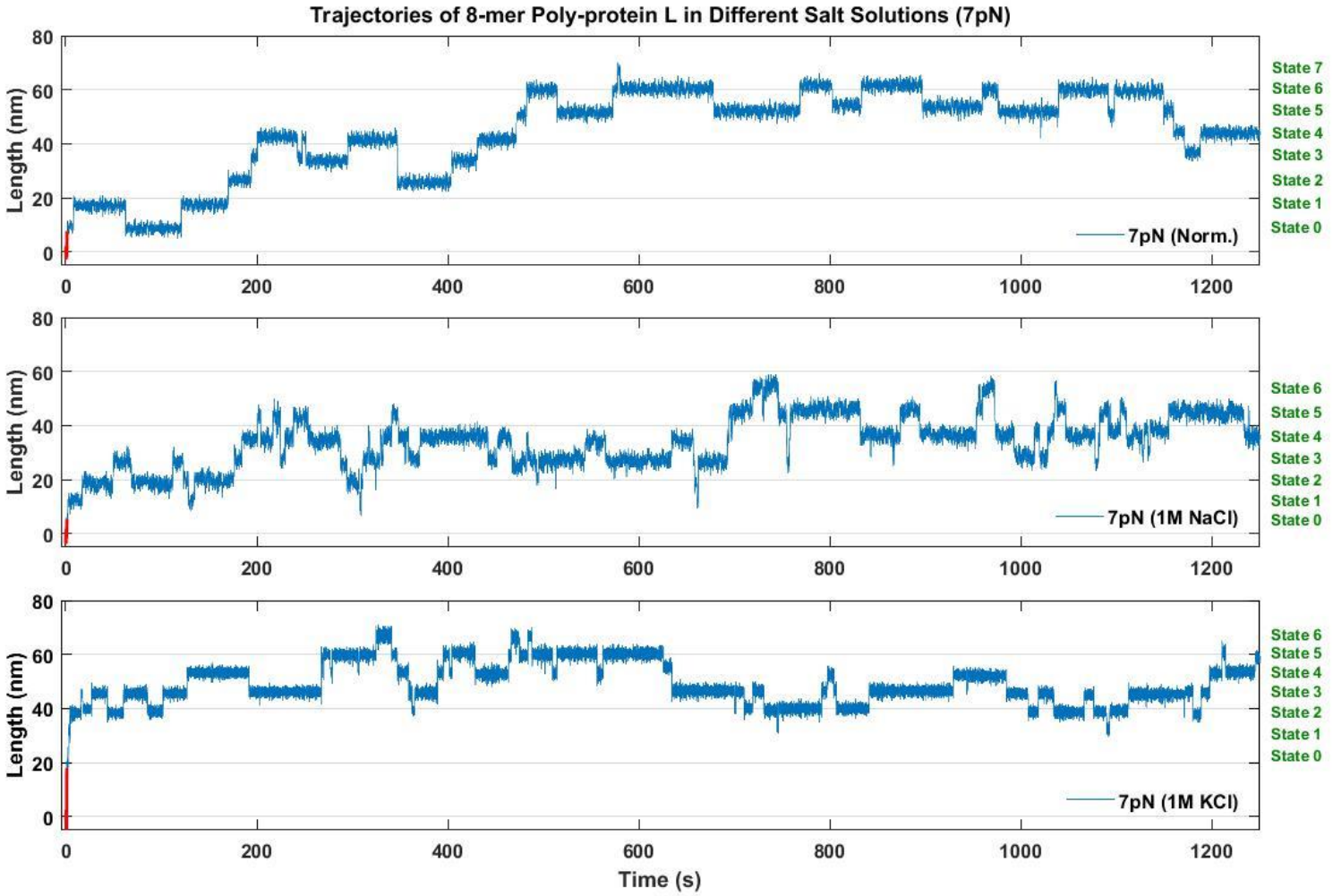

Figure 5.2. Time traces of a single 8-mer poly-protein L in three TRIS-buffered saline solutions at 7 pN. The transition rates are 2.116 ± 0.330, 4.178 ± 0.221 and 3.488 ± 0.207 (1/min) in normal TRIS, TRIS-1M NaCl, and TRIS-1M KCl buffer, respectively.

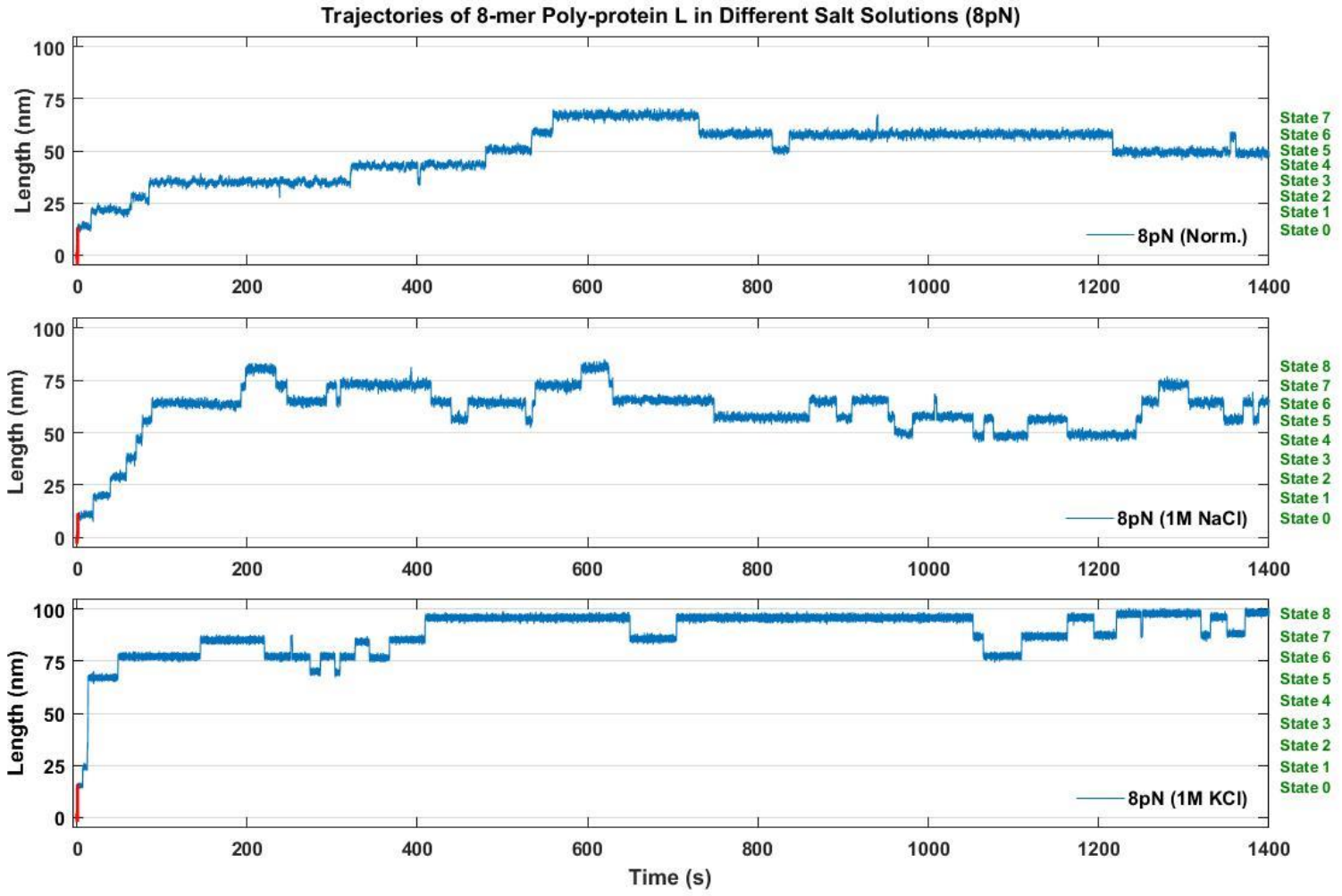

Figure 5.3. Time traces of a single 8-mer poly-protein L in three TRIS-buffered saline solutions at 8 pN. The transition rates are 0.658 ± 0.064, 1.910 ± 0.186 and 1.221 ± 0.136 (1/min) in normal TRIS, TRIS-1M NaCl, and TRIS-1M KCl buffer, respectively.

Table 5.1. Probability of staying at each step of the poly-protein L in normal TRIS buffer, TRIS-1M NaCl buffer, and TRIS-1M KCl buffer at forces of 6 pN, 7 pN, and 8 pN.

TRIS-Normal

Force / # of unfolded proteins	6 pN	7 pN	8 pN
0	0.326 ± 0.107	0.027 ± 0.013	0
1	0.380 ± 0.042	0.095 ± 0.025	0.003 ± 0.003
2	0.214 ± 0.052	0.184 ± 0.062	0.017 ± 0.009
3	0.067 ± 0.025	0.228 ± 0.017	0.046 ± 0.021
4	0.012 ± 0.007	0.214 ± 0.019	0.065 ± 0.022
5	0.001 ± 0.001	0.136 ± 0.029	0.129 ± 0.040
6	0	0.095 ± 0.039	0.305 ± 0.084
7	0	0.020 ± 0.025	0.257 ± 0.055
8	0	0	0.179 ± 0.108

TRIS-1M NaCl

0	0.374 ± 0.119	0.036 ± 0.023	0.004 ± 0.002
1	0.366 ± 0.034	0.106 ± 0.023	0.012 ± 0.004
2	0.211 ± 0.074	0.210 ± 0.037	0.018 ± 0.005
3	0.045 ± 0.023	0.265 ± 0.020	0.040 ± 0.011
4	0.005 ± 0.003	0.217 ± 0.025	0.089 ± 0.032
5	0	0.115 ± 0.023	0.184 ± 0.053
6	0	0.038 ± 0.011	0.275 ± 0.077
7	0	0.012 ± 0.006	0.291 ± 0.088
8	0	0	0.081 ± 0.025

TRIS-1M KCl

0	0418 ± 0.166	0.025 ± 0.011	0.016 ± 0.006
1	0.349 ± 0.061	0.128 ± 0.044	0.011 ± 0.005
2	0.154 ± 0.073	0.262 ± 0.043	0.026 ± 0.007
3	0.069 ± 0.033	0.310 ± 0.028	0.037 ± 0.010
4	0.009 ± 0.006	0.171 ± 0.044	0.056 ± 0.015
5	0	0.092 ± 0.034	0.120 ± 0.033
6	0	0.012 ± 0.006	0.273 ± 0.077
7	0	0.001 ± 0.001	0.301 ± 0.082
8	0	0	0.159 ± 0.068

.

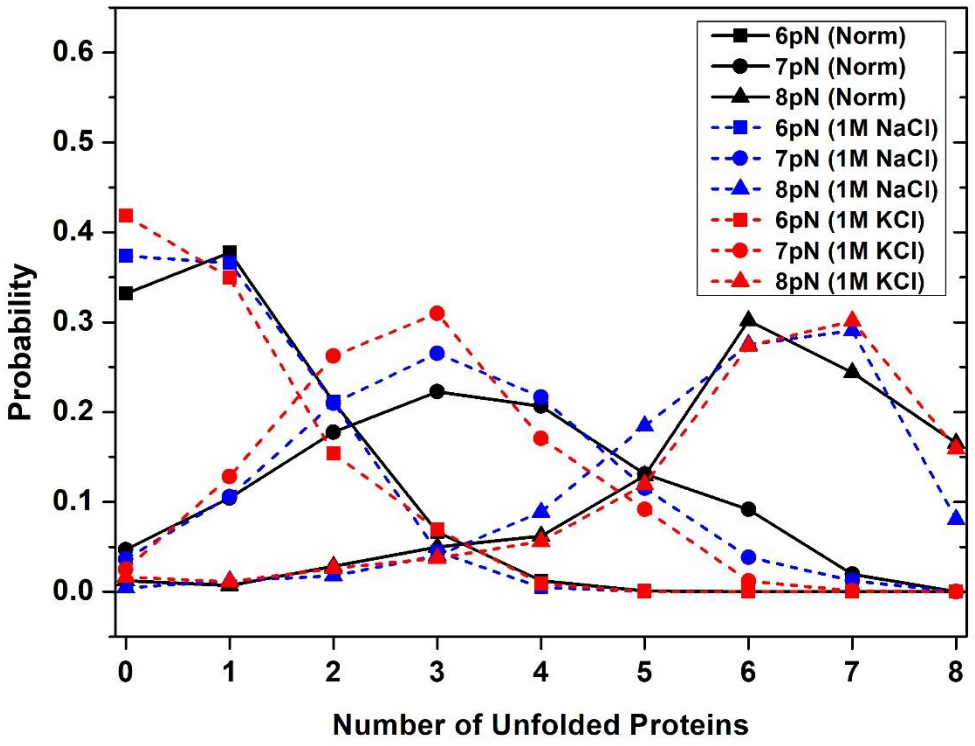

Figure 5.4. Comparison of probability of staying at each state of poly-protein in three TRIS salines under different forces.

As we can see, the poly-protein in TRIS-1M NaCl and that in TRIS-1M KCl buffers basically behave the same way as they do in the normal TRIS buffer. At 6 pN, the poly-proteins are likely to stay at some specific states (state 0 and 1) for all saline solutions. The same goes to other two forces. At 7 pN and 8 pN, the proteins in any of the solutions prefer staying at middle states (state 2-4) and late states (state 6 and 7), respectively. However, the probability ranks may not be the same for all the solutions, for example, at 8 pN, the highest probability in normal TRIS buffer is state 6 rather than state 7 which is the most probable in other two buffers, and the third highest in TRIS-1M NaCl is state 5 instead of the last state in the others. Fortunately, at least the highest probability is always constrained in two consecutive states at each force for the three solutions. The poly-proteins on the whole still follow a trend, that is, in general, with an increase of applied force, the peak shifts from states with few protein L domains unfolded to states with more domains unfolded for all three solutions. We found that, while the probability of poly-protein

L to be found in any state was not affected greatly by addition of salts, we also note that the frequency of jumps between states seems to be salt and force level dependent.

Considering the effect of force on transition rate, we compare time traces of the same salt solution (Figure 5.1-5.3). Obviously, it is more frequently that poly-proteins unfold and refold at low force than at high force no matter what solution it is in. It could be easily proved by calculating the transition rates for the three solutions at each force (see Table 5.2). (Note the unfolding/refolding process of each state is considered the same to simplify the problem.) The numbers with their uncertainties are plotted in Figure 5.5.

On the other hand, when the force is kept the same, the transition frequency of poly-proteins among the three salt solutions are different from each other. The transition rates in normal TRIS are 4.309, 2.116, and 0.658 (1/min) at 6 pN, 7pN, and 8 pN, respectively. When we change the salt solution to TRIS-1M NaCl and TRIS-1M KCl, the rates are respectively increased to 5.394 and 5.588 (1/min) at 6pN, 4.178 and 3.488 (1/min) at 7 pN, and 1.910 and 1.211 (1/min) at 8 pN.

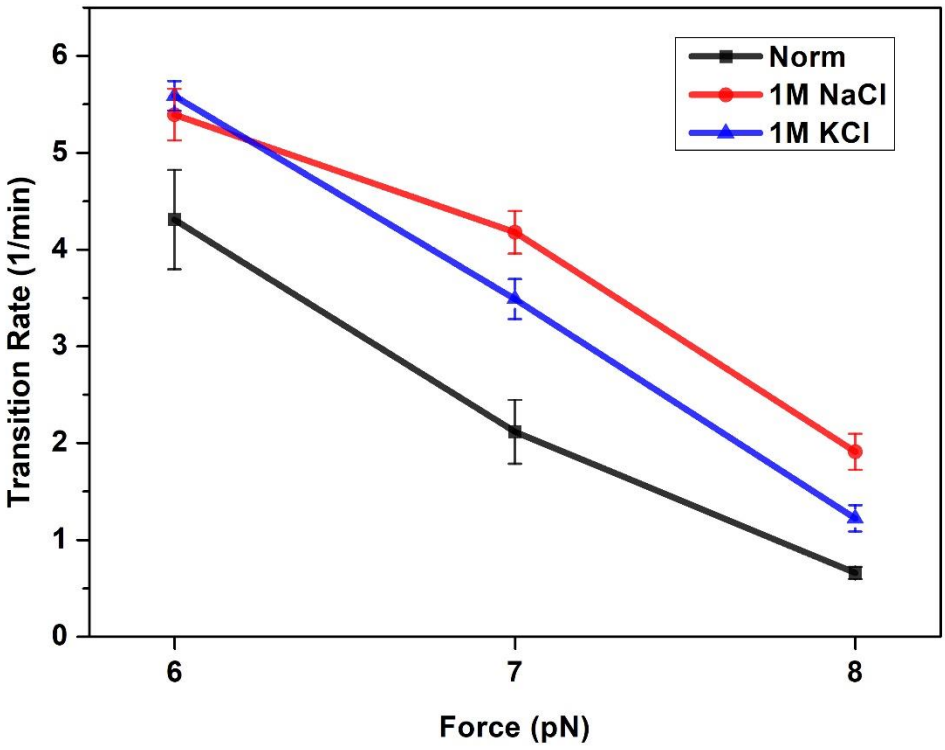

Figure 5.5. The dependency of transition rate of 8-mer poly-protein L on force in three TRIS saline solutions.

Table 5.2. Transition rate between states in the three TRIS-buffered salines at 6pN ,7 pN, and 8 pN and relative transition rate with respect to the rate of normal TRIS buffer.

Rate of Transition (1/min)			
Force (pN) \ TRIS-salt	Normal	1M NaCl	1M KCl
6	4.309 ± 0.513	5.394 ± 0.266	5.588 ± 0.153
7	2.116 ± 0.330	4.178 ± 0.221	3.488 ± 0.207
8	0.658 ± 0.064	1.910 ± 0.186	1.221 ± 0.136
Relative Rate of Transition (a.u.)			
6	1 ± 0.291	1.252 ± 0.138	1.297 ± 0.061
7	1 ± 0.381	1.974 ± 0.234	1.648 ± 0.240
8	1 ± 0.217	3.140 ± 0.664	1.856 ± 0.587

Compared to in the normal TRIS buffer, at each force the poly-proteins have a notable increase in transition rate when they are in TRIS-1M NaCl and TRIS-1M KCl buffers. To further visualize the dependency of transition rate on salt, we defined a "relative transition rate" (see Table 5.2) by individually dividing the transition rates by the rate of the normal TRIS buffer (base). Figure 5.6 shows the relative transition rate of poly-protein in different salt solutions under force. From the figure, we found that the relative transition rates of the two buffers both containing one molar of alkali metal chloride are increased as force increases even though the actual transition rate reacts opposite way. Furthermore, the two saline buffers have totally different slopes. The TRIS-1M NaCl buffer has a slope of 0.826 (1/pN) but the slope of TRIS-1M KCl buffer is only one third of it, which is equal to 0.279 (1/pN). We kept the salt concentrations the same that results in the two solutions having exactly the same amount of positive and negative charges because both salts are of an alkali metal ion and a chloride ion. Hence, it's the salt type (sodium and potassium ions) that causes this difference in transition rate.

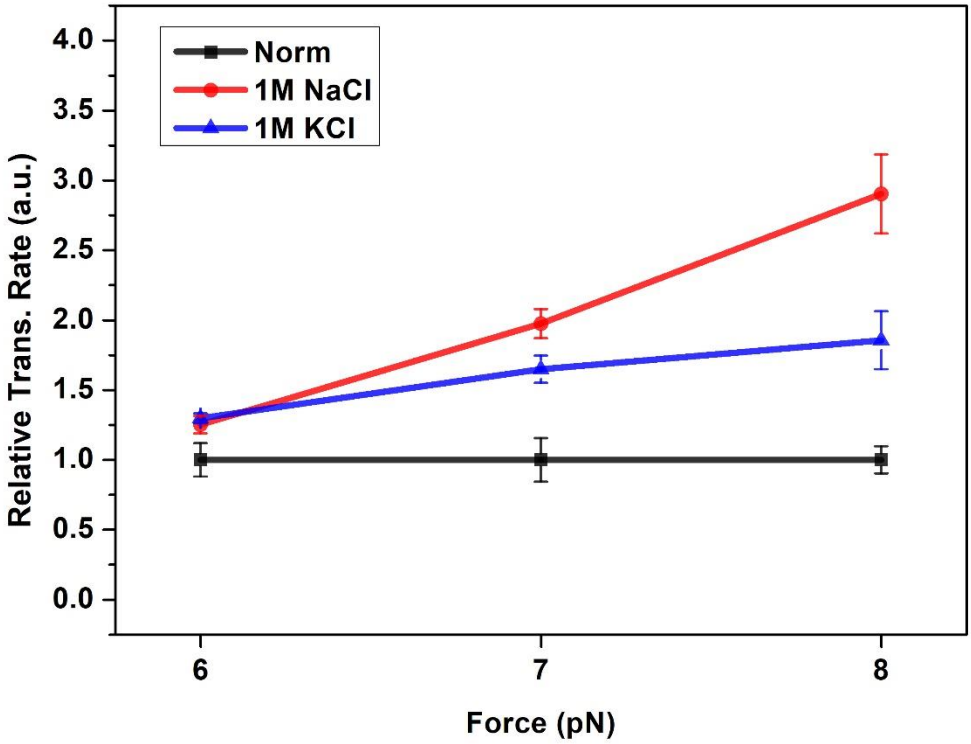

Figure 5.6. Relative transition rate was calculated by dividing the transition rate of each TRIS solution by tbe rate of normal TRIS buffer at each force. It easily shows the trend of increase.

5.3 Discussion

According to Figure 5.4, the poly-protein performance is almost the same for the three types of salt solutions. From Chapter 4, the probability distribution of a poly-protein being at any state is related to the free energy landscape of the poly-protein. It visualizes the free energy of the system by calculating energy gaps between any two states using a Boltzmann distribution. The subtle change among the distributions implies the free energy landscape curves for those three solutions should be similar to each other. Thus, in this project, salt may not cause a huge influence on the overall energy minima.

From the poly-protein extension over time traces, the poly-protein unfolds and refolds more often at low force than high force in any of our solutions. The transition rate (folding and unfolding rates) mainly depends on the energy barrier height between folded and unfolded states according to Kramer's reaction theory, the so-called transition state between the folded and unfolded forms.

A higher transition barrier results in a longer lifetime (slower rate for the poly-protein to overcome the barrier and transition to next state). We can understand this by applying the Bell-Evans-Ritchie model [77, 78]. In this, an external pulling force decreases the free energy of the system linearly with distance. Let's take a two-state protein under force as an example (see Figure 5.7). The energy barrier is lowered by $F \cdot X^{\dagger}$, where F is the external force and $X^{\dagger}$ is the distance from the folded state to the transition state. The lower barrier speeds up the protein to unfold, increasing the forward rate (unfolding rate). However, due to the linear effect, the energy barrier from the other side is increased by $F \cdot (X^{\dagger}+X^{\ddagger})$, where $X^{\ddagger}$ is the distance between the transition state and the unfolded state, which slows down the folding process, accordingly reducing the backward rate (folding rate). Under a force applied, it is easier to unfold but it's harder for the protein to refold. Compare these two effects, the backward effect dominates because the number of folding processes drastically decreases, making the transition rate slower. The impact becomes greater as the force increases. Therefore, the transition rate goes down with increasing force. This applies to all three salt solutions.

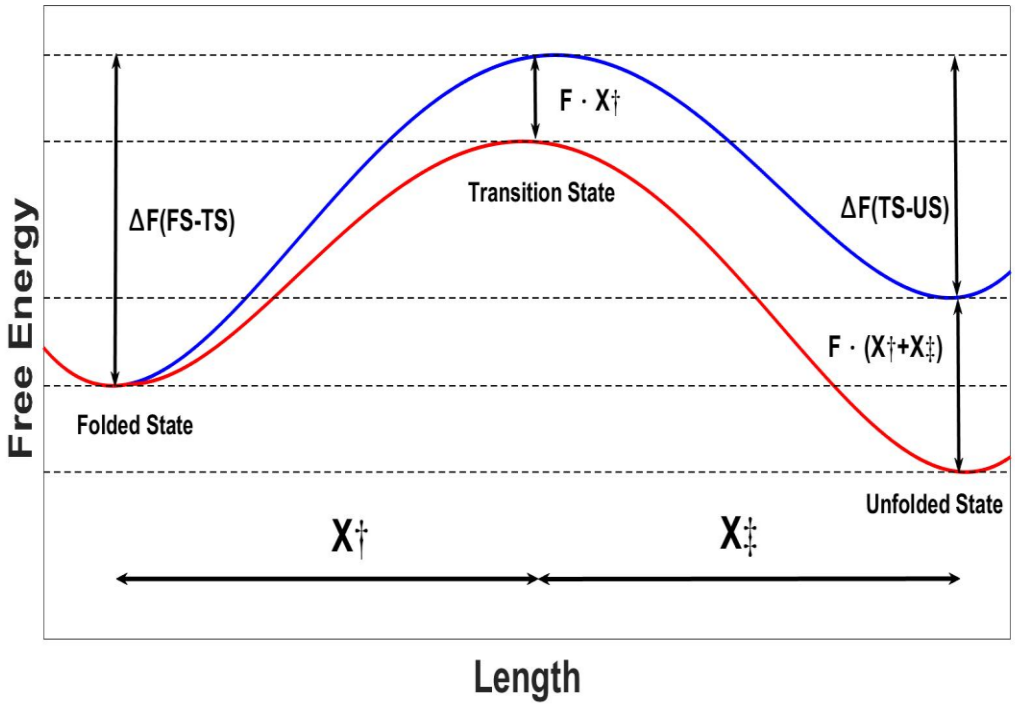

Figure 5.7. Illustration of the change in free energy of a simple two-state protein under an external force applied to it.

As we mentioned above, the transition rates were converted to the relative transition rates to better illustrate how much it has increased at each force. Let's first compare TRIS-normal and TRIS-1M NaCl buffers. When the concentration of NaCl is increased to 1 M, the transition rates are increased by 1.085 (1/min), 2.062 (1/min) and 1.252 (1/min), having the relative transition rates increased by 25%, 97% and 190% at 6 pN, 7pN and 8 pN, respectively. These increments might come from two possibilities: ion-water interactions and ion-protein interactions.

The first and major possibility is salting out effect (ion-water interactions) caused by the increase in salt concentration, that is, an increase in ions to interact with water molecules surrounding the poly-protein, affecting (reducing) interactions between water molecules and the poly-protein. These protein hydration interactions are essential for many biochemical processes, including protein structure (folding and unfolding), protein function and molecular recognition [80-82]. Here we particularly discuss the role of water in protein structure and how it influences the (un)folding dynamics. Proteins have many hydrophobic and hydrophilic amino acids. When dry proteins are exposed to water, the hydrophilic amino acids containing either charged or polar side chains bind to bipolar structured water molecules very quickly through electrostatic interactions (charge-polar or polar-polar interactions) and thereby proteins dissolve in water. The binding of water molecules to the hydrophilic surface of the protein help reorient themselves in an ordered manner to minimize the hydrophobic surfaces to be exposed to water. This effect that drives the hydrophobic groups to form the core of the protein, being protected from aqueous environment by the hydration layer is hydrophobic collapse. This driving force promotes the protein to fold into a three dimensional compact structure. If the effect of the hydration layer is reduced, the protein is no longer stable and easily unfolds. The addition of salt highly affects the protein folding and its solubility in water. When salt is added to the solution, interactions between salt ions and water molecules will take place, creating a charge shielding effect that causes fewer water molecules available to interact with the protein than before. The proteins start to interact with each other and then aggregate and precipitate when the interactions between proteins get stronger. As a result, the proteins become less soluble in water. This process is known as salting out [26, 27]. Besides salting out effect, another possibility to affect the rate is the direct interactions of ions with the protein. There is no scientific evidence that the ion-protein interactions would affect the transition rate in previous literature. However, when plenty of ions get closer to charged

protein, these electrostatic interactions become strong enough and might influence the unfolding/refolding dynamics.

The normal TRIS buffer is not a salt-free solution and the 150 mM NaCl allows for isotonic condition which is good for physiological activities. Proteins under this condition can fold the right way and work properly. However, 1M NaCl should reduce the hydrophilic activities between water particles and proteins. The ions from the salt can compete for interaction with water. Proteins in such high salt concentration are not stable and the unfolding processes would be more frequent. The higher frequency of folding and unfolding means the energy barrier of the transition state is lowered. Unlike the tilting effect from external force, both the folding and unfolding rates are enhanced. The role of high concentration here acts like a catalyst that lowers its activation energy, increasing both forward and backward reaction rates without altering the equilibrium of the reaction. The percentage increase in relative transition rate is higher at high force. We think that the high force can stretch the poly-protein more, giving extra space for the ions to get in to not only enhance the interactions with the poly-protein but also interact with more water molecules that are hard to reach at low force. In conclusion, an increase in salt concentration results in an increase in transition rate because more ion-water interaction and ion-protein interactions occur and this effect (increase in relative transition rate) becomes larger when higher force is applied.

After discussing the impact of salt concentration, we then move on to the comparison between two alkali metal-chloride solutions with the same concentration. When 150 mM NaCl is replaced with 1 M KCl, the transition rates are increased by 1.279 (1/min), 1.372 (1/min) and 0.563 (1/min), having the relative transition rates increased by 30%, 65% and 86% at 6 pN, 7pN and 8 pN, respectively. Compared to performance in TRIS-1M NaCl discussed in the previous paragraph, the TRIS-1M KCl buffer does the same effect on the poly-protein (rate increased at each of forces and higher percentage increase of relative transition rate at high force) but the impact is less (the slope of relative transition rate trend is only one third of that of TRIS-1M NaCl). We attribute this change to the size of ion that affects its ability to form bonds with water molecules. The alkali metals are similar to each other due to having only one electron in the outermost orbit. They tend to lose the outer most electron to form single positively charged ions. When the alkali metal ions are in aqueous solution, the positively charged particles would attract water molecules by forming an M-O (metal-oxygen) bond with the negative pole (oxygen side) of water and those attracted water molecules become a hydration layer around the metal ion. The attraction ability depends on

the bond strength which is highly related to bond length (cation radius + anion radius). In general, the longer the bond the weaker the bond because ions with a large radius have a low charge density which thereby weakens the electrostatic interaction (bond strength) [89]. Shannon provided the effective ionic radii for different coordination numbers [83]. It shows that for the same coordination number the potassium ionic radius is larger than the sodium ionic radius. We only consider the difference between positive ions because the negative ions are the same. Later many studies [84-89] also showed Na-O bond length is shorter than K-O bond length in both experiment and simulation with Na-O length range of 2.34~2.50 Å and K-O length range of 2.65~2.97 Å. These can help explain why TRIS-1M KCl does less impact on poly-protein transition rate because the K-O bond strength is weaker and it reduces the interference on the protein interaction with water. Another possibility is the smaller sodium ions can penetrate into the protein easier to interact directly with the protein than the potassium ions do.

CHAPTER 6. SUMMARY AND FUTURE WORK

6.1 Summary of Experiments

We have constructed a theoretical model for the free energy of the states of an oct-mer poly-protein under the application of differing force loads. We discussed each term of the model and check its validity by nano-manipulation of the poly-protein in a TRIS buffer. Each poly-protein intrinsically has nine states in total, from all protein domains folded to all domains unfolded, and we observed the poly-proteins to transition among the states at forces of 6 pN, 7 pN, and 8 pN. We found out the probability of being each of the nine states and got the probability distribution for each load. The most probable state and its corresponding probability value are state 1, 0.378 ± 0.041, state 3, 0.223 ± 0.016, and state 6, 0.302 ± 0.077 at 6 pN, 7 pN, and 8 pN, respectively. We fit the experimental probability distributions using the force-dependent free energy equation that gives out theoretical probability values. The best fit gives out three fitting parameters, persistence length, contour length, and the unfolding energy, to be 0.4 nm, 18.7 nm, and 6.5 kT. These numbers are in reasonable ranges and thus our model works well.

We then tested the poly-protein performance in three TRIS-saline solutions. We obtain the following important results. First, there is not much difference among the probability distributions of poly-protein in the three solutions. The poly-proteins in each buffer follows that the distribution peak shifts to the state with more unfolded domains as force increases. The overall free energy of each state is the same in all three salt solutions. Second, the transition rate is higher at low force than at high force for all the three salt solutions and it can be well explained by linear energy-tilting effect caused by the application of external force. Third, when the salt (150 mM NaCl) of the normal TRIS buffer is increased to 1M, the (relative) transition rate becomes larger for two reasons. More metal ions can create bonds with water molecules that reduces the interactions between the poly-protein and water. Besides, more electrostatic interactions of ions with the protein might also affect protein stability that increases the (relative) transition rate. Under a high salt concentration, each protein structure is easier to break and the unfolding/refolding processes happen more frequently. The role of high salt concentration acts like a catalyst that lowers the energy barrier between folded and unfolded forms of a protein domain. Furthermore, a high force load can have a larger impact on the increase in relative transition rate. It can extend the protein

more such that the ions can interact with more water molecules that are unavailable to interact with at low force load. It also increase the chances for the ions to interact directly with protein. Last, by a comparison between the two TRIS alkali metal-chloride buffers with the same concentration, the potassium ion has a smaller impact on the relative transition rate. The slope of relative transition rate versus force line for the polyprotein in TRIS-1 M NaCl is three times as large as that in TRIS-1 M KCl. This is because, first, more interactions occur between sodium ions and water molecules than between potassium ions and water due to stronger metal-oxide bond strength, and, second, sodium ions have a smaller size that causes them to penetrate into the protein easier to increase direct interactions with the protein. Thus, the rate is higher in TRIS-1 M NaCl compared to TRIS-1 M KCl.

6.2 Future Work

Our grand goal is to understand the full energy landscape of a folded protein by exploring multi-domain poly-protein under load. At this point, we've obtained some basic results and also constructed a model to explain the poly-protein dynamics under force applied. There still are many interesting projects we can work on in the future. As the short-term goal, we may have a follow-up study of the salt effect. We can try some metal ions with charge +2, such as magnesium ion and calcium ion, or ions with charge +3, such as aluminum ion and chromium ion and compare with previous single positively charged ions. We can keep the concentration of the new salt solution the same as before or the net charge in solution the same. For example, we can make a TRIS buffer with 1M $CaCl_2$ and another TRIS buffer with half of the salt. We compare them to previous results of 1M alkali metal salt solutions and see how these two change the performance. Another possible idea is we can work on just one salt solution but have dense points along the concentration coordinate. We only have two different concentrations (150 mM and 1M) for TRIS-NaCl buffer and we may choose one more concentration in between and also collect data every half of a molar after 1 M until to a super high concentration such as 4 M. This smaller point spacing and wider range can help more accurately get the trend upon the salt concentration and have more information to understand the role of salt in this project.

Throughout this study, we assumed all the protein domains are identical and in Chapter 5, we also considered all unfolding/refolding processes to be the same to simplify the problem, so every single unfolding/refolding was added up to calculate the overall transition rate at each force

load. However, the poly-protein should behave differently at those states because of the nonlinear energy curve that makes all the transition states (barriers) different from each other even though each domain is assumed the same as others in the protein chain. In the energy landscape figure (Figure 4.6), we only figured out the energy minimum of each state, but we haven't determined the transition state (the energy barrier) between each two states. As a mid-term goal, we might play with the unfolding (forward) and refolding (backward) rates at each state and then from the rates of each state, we can work back to get those transition states. To date we don't have a good enough statistics to do so because observations are not long enough which show only a limited number of unfolding and refolding for each state. Therefore, long time traces will be needed so we can check if the protein domains of different states respond the same as each other in the system.

The free energy landscape is sensitive to many factors. It would be very useful if we could describe the energy landscape in multiple "dimensions". In this research, we already have one dimension which is applied force load to show the change in energy landscape. Salt ion and concentration would be the second and third dimensions if we can complete the experiments as mentioned above. As the long-term goal, we are looking to explore as many dimensions as possible. After salt experiment, we are aiming to try various temperatures or pH's in order to more fully explore the folded state energetics.

APPENDIX A. MAGNET POSITION ALIGNMENT

After we set up the MT system, we need to align the system before we collect data to make sure the magnets would move to the right heights by the software made by Julio Fernandez group. The magnets should be aligned to the center of the camera view and also be set to 4 mm above the bottom glass of the chamber under a default force of 4 pN. First of all, mount a low magnification objective on the microscope, adjust the micropositioner to get a clear image of the pair of magnets in the screen and move the magnets slightly to the center of the camera field of view. Second, put a coverslip with a mark on the sample holder and adjust the objective to focus on the mark. After that, we control the micro adjustment to move the magnets down until they touch the coverslip. The focused image would become blurry once they come into contact with the coverglass. Record the position and move the magnets up to the designated height which is 4 mm away from the mark for the 4 pN default force. Then, the alignment for the system has been done.

APPENDIX B. FORCE CHECK

To check if the applied force provided from our MT system is giving the right magnitude, different forces were applied to the poly-protein and the corresponding step sizes were measured and compared to Liu's result (Fernandez group). Figure B. 1 shows our measured step sizes compared to their fitted curve by WLC model given below with the protein L fitting parameters of persistence length ξ of 0.58 nm and contour length L_c of 18.6 nm.

$$F = \frac{k_B T}{\xi}\left[\frac{1}{4}\left(1 - \frac{x}{\Delta L_c}\right)^{-2} - \frac{1}{4} + \frac{x}{L_c}\right], \qquad \text{(B. 1)}$$

where F and x are the applied force and the observed step size, respectively. The observed step sizes with standard errors corresponding to each force are listed in Table B. 1.

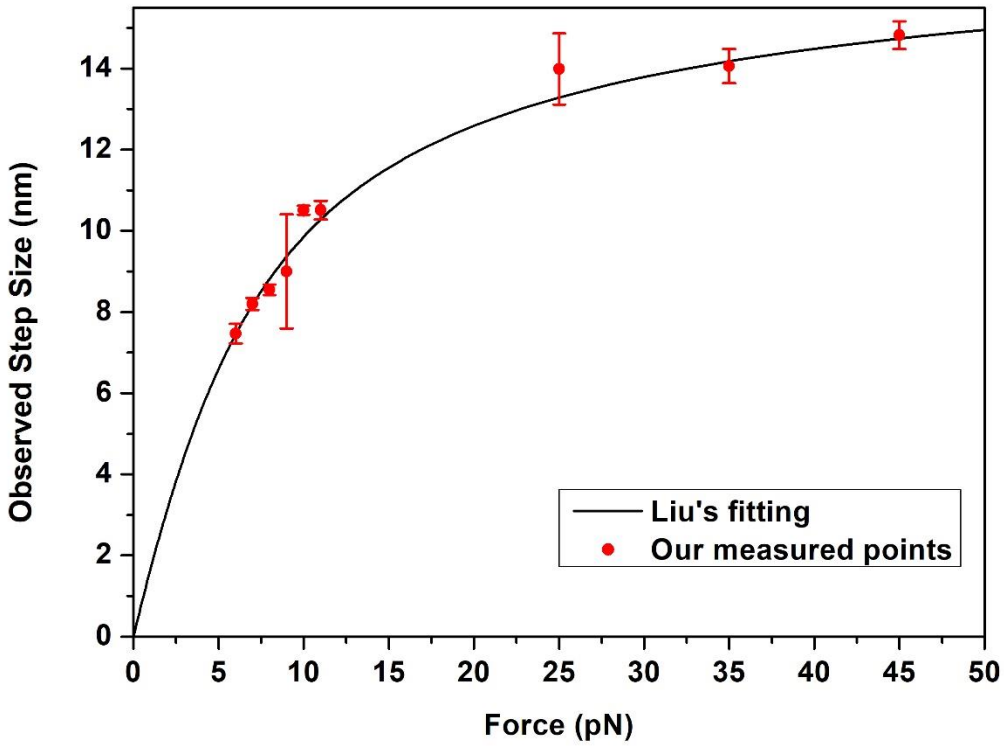

Figure B. 1. A comparison of step size between the results from our group and Liu et al.

Table B. 1

Force (pN)	Step size (nm)
6	7.47 ± 0.24
7	8.20 ± 0.15
8	8.55 ± 0.13
9	9.00 ±1.41
10	10.51 ± 0.11
11	10.51 ± 0.23
25	13.99 ± 0.88
35	14.06 ± 0.42
45	14.82 ± 0.34

REFERENCES

[1] Jackson, S. E. (1998). How do small single-domain proteins fold? *Folding and Design,3*(4). doi:10.1016/s1359-0278(98)00033-9

[2] Grantcharova, V., Alm, E. J., Baker, D., & Horwich, A. L. (2001). Mechanisms of protein folding. *Current Opinion in Structural Biology*, *11*(1), 70–82. doi: 10.1016/s0959-440x(00)00176-7

[3] Privalov, P. L. (1996). Intermediate States in Protein Folding. *Journal of Molecular Biology*, *258*(5), 707–725. doi: 10.1006/jmbi.1996.0280

[4] Plaxco, K. W., Simons, K. T., & Baker, D. (1998). Contact order, transition state placement and the refolding rates of single domain proteins 1 1Edited by P. E. Wright. *Journal of Molecular Biology*, *277*(4), 985-994. doi:10.1006/jmbi.1998.1645

[5] Onuchic, J. N., Luthey-Schulten, Z., & Wolynes, P. G. (1997). THEORY OF PROTEIN FOLDING: The Energy Landscape Perspective. *Annual Review of Physical Chemistry, 48*(1), 545-600. doi:10.1146/annurev.physchem.48.1.545

[6] Eaton, W. A., Muñoz, V., Hagen, S. J., Jas, G. S., Lapidus, L. J., Henry, E. R., & Hofrichter, J. (2000). Fast Kinetics and Mechanisms in Protein Folding. *Annual Review of Biophysics and Biomolecular Structure, 29*(1), 327-359. doi:10.1146/annurev.biophys.29.1.327

[7] Aloy, P., Pichaud, M., & Russell, R. B. (2005). Protein complexes: Structure prediction challenges for the 21st century. *Current Opinion in Structural Biology*, *15*(1), 15-22. doi:10.1016/j.sbi.2005.01.012

[8] Snow, C. D., Sorin, E. J., Rhee, Y. M., & Pande, V. S. (2005). How Well Can Simulation Predict Protein Folding Kinetics and Thermodynamics? *Annual Review of Biophysics and Biomolecular Structure, 34*(1), 43-69. doi:10.1146/annurev.biophys.34.040204.144447

[9] Zhang, Y. (2008). Progress and challenges in protein structure prediction. *Current Opinion in Structural Biology,18*(3), 342-348. doi:10.1016/j.sbi.2008.02.004

[10] Kuhlman, B., & Bradley, P. (2019). Advances in protein structure prediction and design. *Nature Reviews Molecular Cell Biology*, *20*(11), 681-697. doi:10.1038/s41580-019-0163-x

[11] Apic, G., Huber, W., & Teichmann, S. A. (2003). Multi-domain Protein Families and Domain Pairs: Comparison With Known Structures and a Random Model of Domain Recombination. *Journal of Structural and Functional Genomics, 4*(2/3), 67-78. doi:10.1023/a:1026113408773

[12] Bornberg-Bauer, E., Beaussart, F., Kummerfeld, S. K., Teichmann, S. A., & Weiner, J. (2005). The evolution of domain arrangements in proteins and interaction networks. *Cellular and Molecular Life Sciences CMLS, 62*(4), 435-445. doi:10.1007/s00018-004-4416-1

[13] Han, J., Batey, S., Nickson, A. A., Teichmann, S. A., & Clarke, J. (2007). The folding and evolution of multidomain proteins. *Nature Reviews Molecular Cell Biology,8*(4), 319-330. doi:10.1038/nrm2144

[14] Batey, S., Nickson, A. A., & Clarke, J. (2008). Studying the folding of multidomain proteins. *HFSP Journal,2*(6), 365-377. doi:10.2976/1.2991513

[15] Bhaskara, R. M., & Srinivasan, N. (2011). Stability of domain structures in multi-domain proteins. *Scientific Reports, 1*(1). doi:10.1038/srep00040

[16] Vishwanath, S., Brevern, A. G., & Srinivasan, N. (2018). Same but not alike: Structure, flexibility and energetics of domains in multi-domain proteins are influenced by the presence of other domains. *PLOS Computational Biology, 14*(2). doi:10.1371/journal.pcbi.1006008

[17] Tskhovrebova, L., Trinick, J., Sleep, J. A., & Simmons, R. M. (1997). Elasticity and unfolding of single molecules of the giant muscle protein titin. *Nature,387*(6630), 308-312. doi:10.1038/387308a0

[18] Linke, W. A., & Hamdani, N. (2014). Gigantic business: Titin properties and function through thick and thin. *Circulation Research, 114*(6), 1052-1068. doi:10.1161/circresaha.114.301286

[19] Li, H., Linke, W. A., Oberhauser, A. F., Carrion-Vazquez, M., Kerkvliet, J. G., Lu, H., . . . Fernandez, J. M. (2002). Reverse engineering of the giant muscle protein titin. *Nature, 418*(6901), 998-1002. doi:10.1038/nature00938

[20] Rivas-Pardo, J., Eckels, E., Popa, I., Kosuri, P., Linke, W., & Fernández, J. (2016). Work Done by Titin Protein Folding Assists Muscle Contraction. *Cell Reports,14*(6), 1339-1347. doi:10.1016/j.celrep.2016.01.025

[21] Rio, A. D., Perez-Jimenez, R., Liu, R., Roca-Cusachs, P., Fernandez, J. M., & Sheetz, M. P. (2009). Stretching Single Talin Rod Molecules Activates Vinculin Binding. *Science,323*(5914), 638-641. doi:10.1126/science.1162912

[22] Björck L. (1988). Protein L. A novel bacterial cell wall protein with affinity for Ig L chains. *Journal of immunology (Baltimore, Md. : 1950), 140*(4), 1194–1197.

[23] Akerström, B., & Björck, L. (1989). Protein L: an immunoglobulin light chain-binding bacterial protein. Characterization of binding and physicochemical properties. *The Journal of biological chemistry*, *264*(33), 19740–19746.

[24] Kastern, W., Sjöbring, U., & Björck, L. (1992). Structure of peptostreptococcal protein L and identification of a repeated immunoglobulin light chain-binding domain. *The Journal of biological chemistry*, *267*(18), 12820–12825.

[25] Graille, M., Harrison, S., Crump, M. P., Findlow, S. C., Housden, N. G., Muller, B. H., . . . Stura, E. A. (2002). Evidence for Plasticity and Structural Mimicry at the Immunoglobulin Light Chain-Protein L Interface. *Journal of Biological Chemistry, 277*(49), 47500-47506. doi:10.1074/jbc.m206105200

[26] Hofmeister, F. (1888). Zur Lehre von der Wirkung der Salze. *Archiv Für Experimentelle Pathologie Und Pharmakologie*, *24*(4-5), 247-260. doi:10.1007/bf01918191

[27] Hippel, P. H., & Schleich, T. (1969). Ion effects on the solution structure of biological macromolecules. *Accounts of Chemical Research, 2*(9), 257-265. doi:10.1021/ar50021a001

[28] Arakawa, T., & Timasheff, S. N. (1982). Preferential interactions of proteins with salts in concentrated solutions. *Biochemistry, 21*(25), 6545-6552. doi:10.1021/bi00268a034

[29] Arakawa, T., & Timasheff, S. N. (1984). Mechanism of protein salting in and salting out by divalent cation salts: Balance between hydration and salt binding. *Biochemistry*, *23*(25), 5912-5923. doi:10.1021/bi00320a004

[30] Damodaran, S., & Kinsella, J. E. (1981). The effects of neutral salts on the stability of macromolecules. A new approach using a protein-ligand binding system. *The Journal of biological chemistry*, *256*(7), 3394–3398.

[31] Arakawa, T., & Timasheff, S. N. (1984). Protein stabilization and destabilization by guanidinium salts. *Biochemistry, 23*(25), 5924-5929. doi:10.1021/bi00320a005

[32] Arakawa, T., & Timasheff, S. N. (1991). The Interactions of Proteins with Salts, Amino Acids, and Sugars at High Concentration. *Advances in Comparative and Environmental Physiology*, 226-245. doi:10.1007/978-3-642-76226-0_8

[33] Dominy, B. N., Perl, D., Schmid, F. X., & Brooks, C. L. (2002). The Effects of Ionic Strength on Protein Stability: The Cold Shock Protein Family. *Journal of Molecular Biology, 319*(2), 541-554. doi:10.1016/s0022-2836(02)00259-0

[34] Bosshard, H. R., Marti, D. N., & Jelesarov, I. (2004). Protein stabilization by salt bridges: Concepts, experimental approaches and clarification of some misunderstandings. *Journal of Molecular Recognition, 17*(1), 1-16. doi:10.1002/jmr.657

[35] Rief, M. (1997). Reversible Unfolding of Individual Titin Immunoglobulin Domains by AFM. *Science, 276*(5315), 1109-1112. doi:10.1126/science.276.5315.1109

[36] Fernandez, J. M. (2004). Force-Clamp Spectroscopy Monitors the Folding Trajectory of a Single Protein. *Science, 303*(5664), 1674-1678. doi:10.1126/science.1092497

[37] Liu, R., Garcia-Manyes, S., Sarkar, A., Badilla, C. L., & Fernandez, J. M. (2009). Mechanical characterization of Protein L in the low-force regime by electromagnetic tweezers/evanescent nanometry. *Biophysical Journal, 96*(3). doi:10.1016/j.bpj.2008.12.3650

[38] Krueger, M., Koetter, S., Gruetzner, A., Lang, P., & Linke, W. A. (2009). Protein Kinase G Modulates Human Myocardial Passive Stiffness By Phosphorylation Of The Titin Springs. *Biophysical Journal, 96*(3). doi:10.1016/j.bpj.2008.12.2003

[39] Castelmur, E. V., Marino, M., Svergun, D. I., Kreplak, L., Ucurum-Fotiadis, Z., Konarev, P. V., . . . Mayans, O. (2008). A regular pattern of Ig super-motifs defines segmental flexibility as the elastic mechanism of the titin chain. *Proceedings of the National Academy of Sciences, 105*(4), 1186-1191. doi:10.1073/pnas.0707163105

[40] Giganti, D., Yan, K., Badilla, C. L., Fernandez, J. M., & Alegre-Cebollada, J. (2018). Disulfide isomerization reactions in titin immunoglobulin domains enable a mode of protein elasticity. *Nature Communications, 9*(1). doi:10.1038/s41467-017-02528-7

[41] Li, H., Oberhauser, A. F., Fowler, S. B., Clarke, J., & Fernandez, J. M. (2000). Atomic force microscopy reveals the mechanical design of a modular protein. *Proceedings of the National Academy of Sciences, 97*(12), 6527-6531. doi:10.1073/pnas.120048697

[42] Popa, I., Rivas-Pardo, J., Eckels, E., Echelman, D., Badilla, C., Valle-Orero, J. and Fernández, J. (2016). A HaloTag Anchored Ruler for Week-Long Studies of Protein Dynamics. *Journal of the American Chemical Society*, 138(33), pp.10546-10553

[43] Williams, M. C., & Rouzina, I. (2002). Force spectroscopy of single DNA and RNA molecules. *Current Opinion in Structural Biology, 12*(3), 330-336. doi:10.1016/s0959-440x(02)00340-8

[44] Lee, G., Abdi, K., Jiang, Y., Michaely, P., Bennett, V., & Marszalek, P. E. (2006). Nanospring behaviour of ankyrin repeats. *Nature, 440*(7081), 246-249. doi:10.1038/nature04437

[45] Rief, M., Fernandez, J. M., & Gaub, H. E. (1998). Elastically Coupled Two-Level Systems as a Model for Biopolymer Extensibility. *Physical Review Letters, 81*(21), 4764-4767. doi:10.1103/physrevlett.81.4764

[46] Berkovich, R., Garcia-Manyes, S., Klafter, J., Urbakh, M., & Fernández, J. M. (2010). Hopping around an entropic barrier created by force. *Biochemical and Biophysical Research Communications, 403*(1), 133-137. doi:10.1016/j.bbrc.2010.10.133

[47] Chen, H., Yuan, G., Winardhi, R. S., Yao, M., Popa, I., Fernandez, J. M., & Yan, J. (2015). Dynamics of Equilibrium Folding and Unfolding Transitions of Titin Immunoglobulin Domain under Constant Forces. *Journal of the American Chemical Society, 137*(10), 3540-3546. doi:10.1021/ja5119368

[48] Valle-Orero, J., Eckels, E. C., Stirnemann, G., Popa, I., Berkovich, R., & Fernandez, J. M. (2015). The elastic free energy of a tandem modular protein under force. *Biochemical and Biophysical Research Communications*, *460*(2), 434–438. doi: 10.1016/j.bbrc.2015.03.051

[49] Neuman, K. C., & Nagy, A. (2008). Single-molecule force spectroscopy: Optical tweezers, magnetic tweezers and atomic force microscopy. *Nature Methods,5*(6), 491-505. doi:10.1038/nmeth.1218

[50] Svoboda, K., & Block, S. M. (1994). Biological Applications of Optical Forces. *Annual Review of Biophysics and Biomolecular Structure, 23*(1), 247-285. doi:10.1146/annurev.bb.23.060194.001335

[51] Wang, M., Yin, H., Landick, R., Gelles, J., & Block, S. (1997). Stretching DNA with optical tweezers. *Biophysical Journal,72*(3), 1335-1346. doi:10.1016/s0006-3495(97)78780-0

[52] Moffitt, J. R., Chemla, Y. R., Smith, S. B., & Bustamante, C. (2008). Recent Advances in Optical Tweezers. *Annual Review of Biochemistry, 77*(1), 205-228. doi:10.1146/annurev.biochem.77.043007.090225

[53] Clausen-Schaumann, H., Seitz, M., Krautbauer, R., & Gaub, H. E. (2000). Force spectroscopy with single bio-molecules. *Current Opinion in Chemical Biology, 4*(5), 524-530. doi:10.1016/s1367-5931(00)00126-5

[54] Fernandez, J. M., Fisher, T. E., & Marszalek, P. E. (2000). Stretching single molecules into novel conformations using the atomic force microscope. *Nature Structural Biology, 7*(9), 719-724. doi:10.1038/78936

[55] Fotiadis, D. (2002). Imaging and manipulation of biological structures with the AFM. *Micron, 33*(4), 385-397. doi:10.1016/s0968-4328(01)00026-9

[56] Gosse, C., & Croquette, V. (2002). Magnetic Tweezers: Micromanipulation and Force Measurement at the Molecular Level. *Biophysical Journal, 82*(6), 3314-3329. doi:10.1016/s0006-3495(02)75672-5

[57] Vilfan, I. D., Lipfert, J., Koster, D. A., Lemay, S. G., & Dekker, N. H. (2009). Magnetic Tweezers for Single-Molecule Experiments. *Handbook of Single-Molecule Biophysics*, 371-395. doi:10.1007/978-0-387-76497-9_13

[58] Vlaminck, I. D., & Dekker, C. (2012). Recent Advances in Magnetic Tweezers. *Annual Review of Biophysics,41*(1), 453-472. doi:10.1146/annurev-biophys-122311-100544

[59] Sarkar, R., & Rybenkov, V. V. (2016). A Guide to Magnetic Tweezers and Their Applications. *Frontiers in Physics, 4*. doi:10.3389/fphy.2016.00048

[60] Zlatanova, J., & Leuba, S. H. (2003). Magnetic tweezers: A sensitive tool to study DNA and chromatin at the single-molecule level. *Biochemistry and Cell Biology, 81*(3), 151-159. doi:10.1139/o03-048

[61] Celedon, A., Sun, S., Bowman, G., Wirtz, D., & Searson, P. (2009). Magnetic Tweezers Measurement of Single Molecule Torque. *Biophysical Journal, 96*(3). doi:10.1016/j.bpj.2008.12.3651

[62] Kruithof, M., Chien, F., Routh, A., Logie, C., Rhodes, D., & Noort, J. V. (2009). Single-molecule force spectroscopy reveals a highly compliant helical folding for the 30-nm chromatin fiber. *Nature Structural & Molecular Biology,16*(5), 534-540. doi:10.1038/nsmb.1590

[63] Strick, T. R., Kawaguchi, T., & Hirano, T. (2004). Real-Time Detection of Single-Molecule DNA Compaction by Condensin I. *Current Biology,14*(10), 874-880. doi:10.1016/j.cub.2004.04.038

[64] Ribeck, N., & Saleh, O. A. (2008). Multiplexed single-molecule measurements with magnetic tweezers. *Review of Scientific Instruments, 79*(9), 094301. doi:10.1063/1.2981687

[65] Vlaminck, I. D., Henighan, T., Loenhout, M. T., Pfeiffer, I., Huijts, J., Kerssemakers, J. W., . . . Dekker, C. (2011). Highly Parallel Magnetic Tweezers by Targeted DNA Tethering. *Nano Letters, 11*(12), 5489-5493. doi:10.1021/nl203299e

[66] Vries, A. H., Krenn, B. E., Driel, R. V., & Kanger, J. S. (2005). Micro Magnetic Tweezers for Nanomanipulation Inside Live Cells. *Biophysical Journal, 88*(3), 2137-2144. doi:10.1529/biophysj.104.052035

[67] Wang, N., Tytell, J. D., & Ingber, D. E. (2009). Mechanotransduction at a distance: Mechanically coupling the extracellular matrix with the nucleus. *Nature Reviews Molecular Cell Biology, 10*(1), 75-82. doi:10.1038/nrm2594

[68] Wozniak, M. A., & Chen, C. S. (2009). Mechanotransduction in development: A growing role for contractility. *Nature Reviews Molecular Cell Biology,10*(1), 34-43. doi:10.1038/nrm2592

[69] Peterman, E. J., Gittes, F., & Schmidt, C. F. (2003). Laser-Induced Heating in Optical Traps. *Biophysical Journal,84*(2), 1308-1316. doi:10.1016/s0006-3495(03)74946-7

[70] Rasmussen, M. B., Oddershede, L. B., & Siegumfeldt, H. (2008). Optical Tweezers Cause Physiological Damage to Escherichia coli and Listeria Bacteria. *Applied and Environmental Microbiology, 74*(8), 2441-2446. doi:10.1128/aem.02265-07

[71] Lansdorp, B. M., Tabrizi, S. J., Dittmore, A., & Saleh, O. A. (2013). A high-speed magnetic tweezer beyond 10,000 frames per second. *Review of Scientific Instruments,84*(4), 044301. doi:10.1063/1.4802678

[72] Cabiscol, E., Tamarit, J., & Ros, J. (2000). Oxidative stress in bacteria and protein damage by reactive oxygen species. *International microbiology : the official journal of the Spanish Society for Microbiology, 3*(1), 3–8.

[73] Valle-Orero, J., Tapia-Rojo, R., Eckels, E. C., Rivas-Pardo, J. A., Popa, I., & Fernández, J. M. (2017). Proteins Breaking Bad: A Free Energy Perspective. *The Journal of Physical Chemistry Letters,8*(15), 3642-3647. doi:10.1021/acs.jpclett.7b01509

[74] Valle-Orero, J., Rivas-Pardo, J. A., Tapia-Rojo, R., Popa, I., Echelman, D. J., Haldar, S., & Fernández, J. M. (2017). Mechanical Deformation Accelerates Protein Ageing. *Angewandte Chemie, 129*(33), 9873-9878. doi:10.1002/ange.201703630

[75] Frei, B. (1994). Reactive oxygen species and antioxidant vitamins: Mechanisms of action. *The American Journal of Medicine, 97*(3). doi:10.1016/0002-9343(94)90292-5

[76] Pehlivan, F. E. (2017). Vitamin C: An Antioxidant Agent. *Vitamin C*. doi:10.5772/intechopen.69660

[77] Bell, G. (1978). Models for the specific adhesion of cells to cells. *Science, 200*(4342), 618-627. doi:10.1126/science.347575

[78] Evans, E., & Ritchie, K. (1997). Dynamic strength of molecular adhesion bonds. *Biophysical Journal, 72*(4), 1541-1555. doi:10.1016/s0006-3495(97)78802-7

[79] Marko, J. F., & Siggia, E. D. (1995). Stretching DNA. *Macromolecules, 28*(26), 8759-8770. doi:10.1021/ma00130a008

[80] Fogarty, A. C., Duboué-Dijon, E., Sterpone, F., Hynes, J. T., & Laage, D. (2013). Biomolecular hydration dynamics: A jump model perspective. *Chemical Society Reviews, 42*(13), 5672. doi:10.1039/c3cs60091b

[81] Klibanov, A. M. (2001). Improving enzymes by using them in organic solvents. *Nature, 409*(6817), 241-246. doi:10.1038/35051719

[82] Levy, Y., & Onuchic, J. N. (2006). Water Mediation In Protein Folding And Molecular Recognition. *Annual Review of Biophysics and Biomolecular Structure, 35*(1), 389-415. doi:10.1146/annurev.biophys.35.040405.102134

[83] Shannon, R. D. (1976). Revised effective ionic radii and systematic studies of interatomic distances in halides and chalcogenides. *Acta Crystallographica Section A, 32*(5), 751-767. doi:10.1107/s0567739476001551

[84] Mancinelli, R., Botti, A., Bruni, F., Ricci, M. A., & Soper, A. K. (2007). Hydration of Sodium, Potassium, and Chloride Ions in Solution and the Concept of Structure Maker/Breaker. *The Journal of Physical Chemistry B, 111*(48), 13570-13577. doi:10.1021/jp075913v

[85] Maeda, M., & Ohtaki, H. (1975). An X-Ray Diffraction Study of a Concentrated Aqueous Sodium Iodide Solution. *Bulletin of the Chemical Society of Japan, 48*(12), 3755-3756. doi:10.1246/bcsj.48.3755

[86] Ohtomo, N., & Arakawa, K. (1980). Neutron Diffraction Study of Aqueous Ionic Solutions. II. Aqueous Solutions of Sodium Chloride and Potassium Chloride. *Bulletin of the Chemical Society of Japan*, *53*(7), 1789-1794. doi:10.1246/bcsj.53.1789

[87] Azam, S. S., Hofer, T. S., Randolf, B. R., & Rode, B. M. (2009). Hydration of Sodium(I) and Potassium(I) Revisited: A Comparative QM/MM and QMCF MD Simulation Study of Weakly Hydrated Ions. *The Journal of Physical Chemistry A, 113*(9), 1827-1834. doi:10.1021/jp8093462

[88] Tongraar, A., Liedl, K. R., & Rode, B. M. (1998). Born−Oppenheimer ab Initio QM/MM Dynamics Simulations of Na+and K+in Water: From Structure Making to Structure Breaking Effects. *The Journal of Physical Chemistry A, 102*(50), 10340-10347. doi:10.1021/jp982270y

[89] Mähler, J., & Persson, I. (2011). A Study of the Hydration of the Alkali Metal Ions in Aqueous Solution. *Inorganic Chemistry, 51*(1), 425-438. doi:10.1021/ic2018693

VITA

Jian-Yu Chen was born in Taipei, Taiwan on September 6 in 1986. He became interested in science and math at his middle school age. After several years of scientific exploration in high school, he decided to study physics as the major at a university. He went to department of physics at National Taiwan Normal University to start the university life in 2005 and received the bachelor's degree of science in 2009. During this period, he was given plenty of scientific knowledge and trainings that make him qualified for graduate studies in the future and at the same time he took teacher education program because he wanted to spread physics knowledge to others using a simple and understandable way. After graduating from NTNU, he became a student teacher practicing his teaching skills for physics at Taipei Municipal Jianguo High School. After that, he went to graduate institute of applied physics at National Taiwan University in 2010 to pursue his master's degree, focusing on his interest in optoelectronics, specializing in organic solar cells under the supervision of Prof. Yang-Fang Chen. Two years later, he completed a thesis entitled "High Performance of Organic/ZnO-nanorod Hybrid Solar Cells Assisted by Conductive Small Molecules" and he was awarded Dean's Award (Excellent Thesis Award). After a year of compulsory substitute military service, he chose to return to academia to continue his academic career.

In 2014, Jian-Yu got an admission letter from the department of physics and astronomy at Purdue University and he then moved to West Lafayette, Indiana, USA to begin the doctoral program. During the first and second year, he passed the qualifying exam and shuffled in groups to find out his research interest. He officially joined Prof. Ken P. Ritchie lab in the fall of 2016, starting research in "Single Molecule Biophysics". He has been studying the dynamics of poly-protein L under mechanical force for years using a single-molecule nano-manipulation tool: magnetic tweezers built with his advisor. Under Ken's kindly and helpful guidance, he has made good progress and his research results are good enough to be published in SCI journals. After graduation, he will go back to Taiwan and find a research position in industry to dedicate what he learned from the USA to his lovely home country.